THEORETICA CHIMICA ACTA

Theoret. Chim. Acta (Berl.) 60, 233–268 (1981)

Electron Correlation in Weakly Coupled Transition Metal Dimers: Bimetallocenylenes and Bimetallocenes

Michael C. Böhm

Institut für Organische Chemie der Universität, Im Neuenheimer Feld 270, D-6900 Heidelberg, Federal Republic of Germany

The Hartree–Fock (HF) instabilities in a series of bimetallocenes (**1**) and bimetallocenylenes (**2**) with Fe, Co, Ni and Cr as $3d$ centers have been investigated by means of a semiempirical INDO Hamiltonian. The HF picture is only valid in the case of the iron dimers. Strong correlation effects are encountered in the Co, Ni and Cr complexes. The necessary conditions for singlet, non-singlet (triplet) and non-real variations of the HF orbitals are discussed in detail. Singlet fluctuations are the result of intraatomic angular correlation (short-range) at each $3d$ center. The violation of the spin symmetry corresponds to a long-range interaction between the transition metal centers. Only for MOs with large $3d_{xz}$ amplitudes there exists a channel for the interatomic spin decoupling. Consequences for polymetallocenes are shortly discussed.

Key words: Hartree–Fock instabilities – Electron correlation in binuclear transition metal compounds – INDO calculations.

1. Introduction

In recent years various attempts have been undertaken to synthesize organometallic polymers with conducting or semiconducting properties [1, 2]. Two general types of such species are displayed below (**A** and **B**); in systems of the type **A** transition metal centers are directly coupled. In **B** a periodical alteration between $3d$ centers and conjugated organic fragments is encountered. Krogmann's salt **C** is one of the classical representatives for the **A** type polymers [3]. Within the alternating infinite chains **B**, poly-decker sandwich compounds **D** and polymetallocenes **E** have received much interest [4–7]. In the case of the

0040-5744/81/0060/0233/$07.20

multiple-stacked species synthetic routes at the present time are limited to 3 metal 3*d* centers [4, 5]. Polyferrocenes **E** and various derivatives of the Fe parent on the other hand have been studied in large detail in recent years [6, 7].

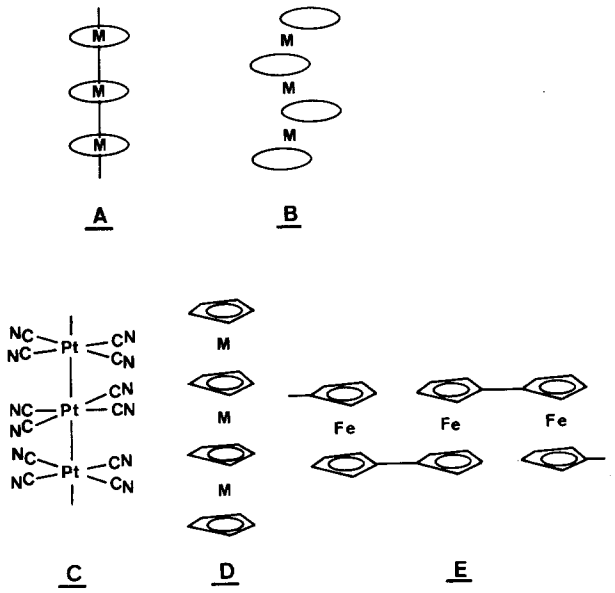

The conducting properties of such systems are determined by characteristic quantities of the charge carrier dynamics [8], e.g. the effective mass tensor, the mobility tensor or the velocity of the particles and their mean free path. Theoretical calculations of these properties must be either performed in the framework of band-structure procedures or by methods taking into account an activated type of transport between localized states (electron hopping) [9]. The validity of such model-assumptions has to be tested by comparison with experimental data.

The coexistence of localized states and delocalized band-structures are well known in solid state physics, and their mutual interconversion is commonly called "electronic phase transition" [10, 11]. Due to the pioneering work of Slater [12] and Mott [13] it is by now a common knowledge that the existence of electronic phase transitions is a result of electron correlation.

The quantitative determination of correlation effects in organic and organometallic polymers is a difficult task and is restricted to simple model systems [14, 15]. As a consequence of the enormous computational difficulties encountered in band-structure calculations on systems like **C** to **E** the available tight-binding calculations are limited to one-electron models of the Wolfsberg–Helmholtz type [16–18]. Neither Hartree–Fock (HF) SCF computations nor calculations beyond the one-particle HF picture under the inclusion of many-body interactions have been performed for the aforementioned polymer species.

On the other hand we have demonstrated in recent publications [19–21] that it is possible to investigate the importance of electron correlation, the type and the range of many-body interactions as well as violations of spatial and spin symmetry beyond the HF approximation, on discrete dimeric or trimeric building-stones of the corresponding infinite chains. Theoretical framework for such an approach are the Thouless instability conditions [22], e.g. the stability of the HF wave function against orbital fluctuations. The intimate correspondence between theoretical findings observed for discrete molecular clusters and polymers constructed from these subunits has been pointed out by Whangbo [23]. To a large degree it is possible to transfer and extrapolate computational results and physical models from the molecular systems to the infinite frameworks.

In the present publication we want to investigate the importance of electron correlation in the dimeric units of polymetallocenes **E** (bimetallocenes **1**) and the related bimetallocenylenes **2**.

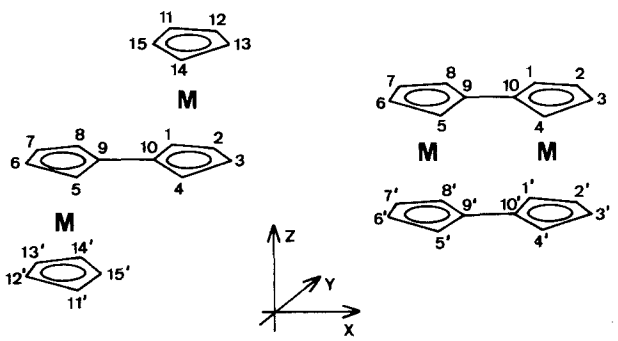

M = Fe	1a		M = Fe	2a
Co	1b		Co	2b
Ni	1c		Ni	2c
			Cr	2d

In detail we have studied the iron derivatives **1a** and **2a** which are known for a long time [7]. The Co and Ni complexes **1b/2b** and **1c/2c** have been synthesized recently [24]. The dimeric compounds are diamagnetic at room temperature indicating paired spins of the 3*d* electrons. A diamagnetic ground state is also found in the Cr derivative of the bisfulvalene family **2d** [25]. The investigation of the stability of the HF approximation in the closed shell systems **1** and **2** seems of large inferest as we have demonstrated that SCF calculations on cationic hole-states of **1a** and **2a** converge into states with localized 3*d* orbitals [26, 27]. The symmetry adapted HF determinants represent no minimum in the MO space.

The computational framework of the present study is based upon a recently developed INDO algorithm for transition metal compounds designed to reproduce the predictive capability of *ab initio* calculations of high sophistication [28].

2. Theory

The conditions for HF instabilities were originally derived by Thouless [22]. Čižek and Paldus have reformulated the eigenvalue problem of the HF fluctuations and introduced the method for quantum chemical applications [29]. Detailed derivations of the corresponding working equations can be found in several references [29–32]. Therefore only a short summary of the theoretical background is given. A detailed analysis of instability types and conditions in transition metal dimers is given in Ref. 21.

According to Thouless the stability of the HF ground state determinant $|\phi_0\rangle$ is related to the real nature of the orbital fluctuations calculated by means of time-dependent HF theory (random phase approximation, RPA) [22]. It is assumed that an arbitrary Slater determinant $|\phi\rangle$ in the neighborhood of $|\phi_0\rangle$ may be constructed by spin orbitals $|\phi_k\rangle'_\sigma$ which are related to the MOs of $|\phi_0\rangle$, $|\phi_k\rangle_\sigma$, via Eq. (1):

$$|\phi_k\rangle'_\sigma = |\phi_k\rangle_\sigma + \sum_{l=N+1}^{\infty} c_{kl}|\phi_l\rangle_{\sigma'} \tag{1}$$

c_{kl} is the mixing amplitude between the kth occupied MO of $|\phi_0\rangle$ and the lth virtual orbital. The spin orbitals $|\phi_k\rangle_\sigma$ are given as product of a space part ($|\phi_k\rangle$) and the spin function $|\sigma(s)\rangle$.

$$\begin{aligned} &|\phi_k\rangle_\sigma = |\phi_k\rangle|\sigma(s)\rangle \\ &\sigma(s) = \begin{matrix}\alpha \\ \beta\end{matrix} \quad \text{spin.} \end{aligned} \tag{2}$$

The unitary transformations in Eqs. (3)–(6) allow the formulation of an eigenvalue problem for HF fluctuations in the basis of space orbitals.

$$c^1_{kl} = \frac{1}{\sqrt{2}}(c_{k\alpha l\alpha} + c_{k\beta l\beta}) \tag{3}$$

$$c^3_{kl} = \frac{1}{\sqrt{2}}(c_{k\alpha l\alpha} - c_{k\beta l\beta}) \tag{4}$$

$$c^{3'}_{kl} = \frac{1}{\sqrt{2}}(c_{k\beta l\alpha} + c_{k\alpha l\beta}) \tag{5}$$

$$c^{3''}_{kl} = \frac{i}{\sqrt{2}}(c_{k\beta l\alpha} - c_{k\alpha l\beta}). \tag{6}$$

Eq. 3 is associated with singlet variations of the HF determinant, Eq. (4)–(6) correspond to non-singlet (triplet) excitations, with real amplitudes (4) and (5) and a complex amplitude in Eq. (6). The stability condition based on RPA is given by the eigenvalue problems (7) and (8) for the excitation energies ${}^{1,3}\lambda$ of the N electron system.

$$[{}^1X + {}^1Y]C^1 = {}^1\lambda C^1 \tag{7}$$

$$[^3X + {}^3Y]C^3 = {}^3\lambda C^3. \tag{8}$$

Eq. (7) represents the singlet variations and (8) is the eigenvalue problem of non-singlet (triplet) fluctuations. $^{1,3}X$ is the CI matrix containing singly excited configurations on the diagonal and the off-diagonal cross-terms. $^{1,3}Y$ symbolizes the interaction matrix between the HF ground-state $|\phi_0\rangle$ and doubly excited configurations. If the MOs are expressed in the diagonal basis of the canonical molecular orbitals, ϕ_k, the matrix elements of X and Y are defined in Eq. (9) and (10).

$$^{1,3}X_{kl,jm} = (\varepsilon_l - \varepsilon_k)\delta_{kj}\delta_{lm} + (kl, jm) - (kj, lm) \pm (kl, jm) \tag{9}$$

$$^{1,3}Y_{kl,jm} = (kl, jm) - (km, jl) \pm (kl, jm). \tag{10}$$

The upper signs correspond to the singlet fluctuations (^1X, ^1Y), and the lower ones to the triplet variations (^3X, ^3Y). The MO indices j and k refer to molecular hole-states while l and m are associated with the particle-set. The ε_ks stand for the energies of the canonical molecular orbitals of the restricted HF eigenvalue problem (11) where

$$F|\phi_k\rangle = \varepsilon_k|\phi_k\rangle \tag{11}$$

F symbolizes the Fock-operator. The electron–electron interaction integrals in the ϕ_k basis are defined in (12).

$$(kj, lm) = \left\langle \phi_k(1)\phi_j(1)\left|\frac{1}{r_{12}}\right|\phi_l(2)\phi_m(2)\right\rangle. \tag{12}$$

Due to the identity (13) a third eigenvalue problem (14) can be formulated with complex orbitals $i|\phi_k\rangle_\sigma$. The wave functions of (14) are imaginary for the real amplitudes (3)–(5), and real for the imaginary amplitude (6).

$$^1X - {}^1Y = {}^3X - {}^3Y \tag{13}$$

$$[^1X - {}^1Y]C^c = [^3X - {}^3Y]C^c = {}^c\lambda C^c. \tag{14}$$

The global stability of the HF ground state $|\phi_0\rangle$ can be expressed as min ($^1\lambda$, $^3\lambda$, $^c\lambda) > 0$. If $^1\lambda > 0$, the HF wave function corresponds to a local minimum with respect to variations that violate the spatial and spin symmetry retaining the real character of $|\phi_0\rangle$. $^1\lambda < 0$ on the other hand is associated with singlet fluctuations (spin symmetry is conserved) of the space functions. If ϕ_k and ϕ_l correspond to different irreducible representations the symmetry properties of the new orbitals $|\phi_k\rangle'$ are broken (e.g. Löwdin's symmetry dilemma [33]). The molecular orbital wave functions do not transform according to the irreducible representations of the molecular point group. This type of solution is called charge density wave (CDW) [31, 34].

The non-singlet (triplet) instability is the result of $^3\lambda < 0$; here at least one unrestricted solution is lower in energy than the spin paired RHF determinant. The violation of the spatial symmetry depends on the irreducible representations of ϕ_k and ϕ_l. The amplitudes of Eq. (4) lead to a wave function which is an

eigenfunction of S_z (z-component of the total spin S) but not of S^2. $c_{kl}^{3'}$ and $c_{kl}^{3''}$ in (5) and (6) are neither an eigenfunction of S_z nor of S^2; the HF flucutuations defined in (6) correspond to wave functions that are no longer real. The solutions of the non-singlet instability problem are called spin density waves (SDW) and have been discussed for the first time by Overhauser in an electron gas [35].

Eq. (14) defines the stability condition against non-real (complex) variations of the orbital wave functions. Due to the identity (13) there are four complex solutions indicating the degeneracy of a singlet and non-singlet instability.

The marking point $\lambda = 0$ separating stable ($\lambda > 0$) and unstable ($\lambda < 0$) HF solutions has only a strict, limiting function if all singly and doubly excited configurations are considered in the eigenvalue problems (complete CI). In the case of the complex species **1a–1c** and **2a–2d** this complete configuration interaction is beyond current computational capacities. Only a limited set of singly and doubly excited configurations can be taken into account (limited CI). Therefore a sharp instability threshold dividing stable and unstable HF solutions cannot be defined a priori. Instead using the $\lambda = 0$ mark, a classification scheme should be employed that is of an extended, more general character. Obviously the influence of electron correlation is reduced with enlarged positive excitation energies (as $\lambda \to \infty$, many-body contributions $\to 0$). In the case of negative roots the HF approximation dramatically breaks down, and new solutions of the SDW and CDW type are encountered. Eigenvalues in the vicinity of $\lambda = 0$ (i.e. $0 < \lambda < \eta$, where η is a small positive number) indicate the significant importance of electron correlation although the HF ground state $|\phi_0\rangle$ is not unstable with respect to orbital fluctuations. The HF one-determinant $|\phi_0\rangle$ nevertheless is no sufficient approximation for the electronic ground state of the system under investigation.

In Ref. 21 we have discussed in detail the necessary conditions of the various instability types as well as the physical nature of the correlation processes encountered in weakly coupled species with $3d$ centers related due to symmetry. In poly-decker sandwich compounds we have demonstrated that singlet instabilities are the result of a superposition of angular and left–right correlation [36]. Both many-body interactions contribute with comparable magnitude to the net HF fluctuations. The angular part is predominantly of intraatomic type ($3d$ centers) and corresponds to an orbital excitation between $3d$ AOs of different z components of the magnetic quantum number. Schematically this can be written as in Eq. (15) where only the $3d$ contributions to the MOs are displayed.

$$(3d_i) \to (3d_j) \tag{15}$$

$$i, j = z^2, xz, yz, x^2 - y^2, xy \tag{16}$$

$$i \neq j. \tag{17}$$

The second correlation type in poly-decker compounds is the interatomic left–right coupling transmitted via the organic ligand system. This interaction consists of an electron-hole pair $\phi_k | \phi_l$ with an even and an odd MO wave function. One

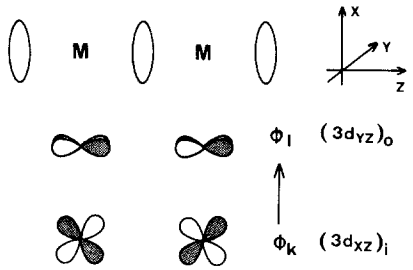

Fig. 1. Schematical representation of an electron-hole pair $\phi_l | \phi_k$ in a triple-decker sandwich where angular and left–right correlation are effectively coupled

of the $3d$ linear combinations must be an in-phase (bonding) combination, and the other must be an out-of-phase (antibonding) one. Singlet fluctuations furthermore are possible only if a second orbital excitation with the corresponding properties (z component of the magnetic quantum number and phase relation) couples strongly to the first HF fluctuation via the off-diagonal elements of the singlet eigenvalue problem. A general orbital excitation in a triple-decker compound where both correlation types are present is shown below and is displayed schematically in Fig. 1 where

$$(3d_{xz})_i \rightarrow (3d_{yz})_o \tag{18}$$

i symbolizes an in-phase, and o an out-of-phase combination. (18) must be coupled to a nearby HF fluctuation of the type shown in Eq. (19).

$$(3d_{yz})_o \rightarrow (3d_{xz})_i. \tag{19}$$

Non-singlet (triplet) instabilities are the result of a spin decoupling within an i/o or bonding/antibonding MO pair with large $3d$ contributions. Schematically an orbital excitation leading to an UHF wave function is shown below:

$$(3d_{xz})_i \rightarrow (3d_{xz})_o. \tag{20}$$

In contrast to singlet fluctuations, the non-singlet excitation is determined predominantly by the diagonal elements of the eigenvalue problems, since small energy gaps and large exchange integrals (kl, kl) for the electron-hole pair $\phi_k | \phi_l$ favour the occurrence of triplet variations. In the case of binuclear complexes with $3d$ centers related due to the molecular symmetry this type of correlation is always of long-range, interatomic character. The computational results of our recent studies have shown that the non-real instabilities in transition metal compounds are similar to the singlet excitations (magnitude of the λ values, eigenvectors of the instability problem) [21].

3. Computational Method

Computational framework of the present study is a recently developed INDO model for transition metal compounds [28]. This method has been designed to reproduce results of *ab initio* calculations of high sophistication as well as experimental observables (ionization potentials, excitation energies, geometries, dipole moments) with sufficient precision at low computational cost. In the case

of the two iron dimers **1a** and **2a**, the effective ZDO-Hamiltonian allowed the evaluation of vertical ionization potentials by means of ΔSCF and "Transition Operator" calculations with high accuracy [26, 27]. The PE spectra of the iron complexes have been asigned unambiguously in the lower energy region by means of the INDO procedure and have been checked by experimental correlation techniques. The experience gained from the $3d$ complexes **1a** and **2a** [26, 27] as well as various other INDO studies on the electronic structure of transition metal compounds [37–39] suggests that our semiempirical procedure is a suitable tool to rationalize the validity of the HF approximation in the dimers **1** and **2** on a substantial computational level.

The INDO calculations on the two series **1** and **2** were performed on X-ray diffraction data or on extrapolated geometries from the corresponding monomer species. The X-ray data on the biferrocene complex **1a** indicate a trans conformation of the two ferrocene units [40]. Experimentally a small deviation from C_{2h} symmetry has been detected, i.e. the orientation between the fulvalene bridge and the cyclopentadienyl (cp) rings lies between the eclipsed and staggered conformation. To simplify the theoretical analysis the staggered C_{2h} orientation has been used. The Fe centers in **1a** are separated by 5.08 Å and the separation between the $3d$ center and the π-planes amounts to 1.65 Å. In the bisfulvalene derivative **2a** a FeFe separation of 3.98 Å has been obtained [41]. The mean FeC distance is 2.06 Å. The dimers of the series **2** belongs to the point group D_{2h}.

In the case of the Co, Ni and Cr derivatives **1b**, **1c**, **2b**, **2c** and **2d**, the geometries of the ligands correspond to those of the iron derivatives. The metal carbon distances were taken from the various metallocenes [42]. Mean interatomic $3d$

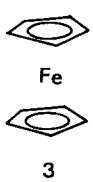

3

carbon separations in the Co, Ni and Cr dimers of 2.20, 2.12, and 2.17 Å have been used. The $3d$ centers in series **2** have a common separation of 3.98 Å. In the bimetallocene compounds **1a**, **1b** and **1c** the distance between the $3d$ sites are 5.08, 5.19 and 5.33 Å, respectively. The interaction matrix in the instability problems corresponds to an eigenvalue problem with 16 hole- and 9 particle-states; the orbital fluctuations were selected on the basis of the diagonal elements of a 20×20 excitation scheme. From this diagonal array 16 hole- and 9 particle-states have been taken into account leading to the smallest excitation energies.

4. A Common MO Model for the Bimetallocenes and Bimetallocenylenes

The electronic structure of the two binuclear transition metal series **1** and **2** can be derived on the basis of the MO sequence of the corresponding metallocenes, e.g. ferrocene **3**. The bonding interactions in cp_2Fe have been analyzed in large

detail both by means of semiempirical LCAO calculations [43] and by means of *ab initio* procedures [44]. The $3d$ AOs $3d_{z2}$, $3d_{x2-y2}$ and $3d_{xy}$ do not interact strongly with ligand orbitals and form a set of MOs with predominant $3d$ character of the symmetry e_{2g} ($3d_{x2-y2}$, $3d_{xy}$) and a_{1g} ($3d_{z2}$). In cp_2Mn a crossing of the MO sequence e_{2g}/a_{1g} takes place. On the left side in the $3d$ series a_{1g} is found on top of e_{2g}, but on the right side this ordering is exchanged [45]. The $3d$ AOs $3d_{xz}/3d_{yz}$ are destabilized by ligand π- and σ-orbitals and stabilized by ligand π^* functions (symmetry: e_{1g}).

In the bimetallocene and bimetallocenylene series these functions are combined to a bonding (B) and antibonding (AB) linear combination. The ten MOs transform according to the following irreducible representations of the point group C_{2h} and D_{2h}:

	C_{2h}	D_{2h}
$(3d_{z2})_B = N(3d_{z2}+3d_{z2})$	a_g	a_g
$(3d_{z2})_{AB} = N(3d_{z2}-3d_{z2})$	b_u	b_{3u}
$(3d_{x2-y2})_B = N(3d_{x2-y2}+3d_{x2-y2})$	a_g	a_g
$(3d_{x2-y2})_{AB} = N(3d_{x2-y2}-3d_{x2-y2})$	b_u	b_{3u}
$(3d_{xy})_B = N(3d_{xy}-3d_{xy})$	a_u	b_{2u}
$(3d_{xy})_{AB} = N(3d_{xy}+3d_{xy})$	b_g	b_{1g}
$(3d_{yz})_B = N(3d_{yz}+3d_{yz})$	b_g	b_{3g}
$(3d_{yz})_{AB} = N(3d_{yz}-3d_{yz})$	a_u	a_u
$(3d_{xz})_B = N(3d_{xz}-3d_{xz})$	b_u	b_{1u}
$(3d_{xz})_{AB} = N(3d_{xz}+3d_{xz})$	a_g	b_{2g}

N = normalization constant

The irreducible representations correspond to the coordinate system displayed in Sect. 1.

The energy ordering of the $3d_{xz}/3d_{yz}$ linear combination in **1** and **2** depends critically on the coupling with the π^* acceptor orbitals of the fulvalene and cp ligands. The four π^* MOs of $(C_{10}H_8)^{2-}$ are displayed in Fig. 2. $\pi^*(b_{1u})$ is the lowest virtual MO of the fulvalene dianion, $\pi^*(b_{2g})$ and $\pi^*(a_u)$ are nearly degenerate, and $\pi^*(b_{3g})$ corresponds to the highest acceptor MO [46]. On the basis of qualitative perturbational arguments it is expected that $(3d_{xz})_B$ is the lowest particle MO of the binuclear iron complexes, $(3d_{yz})_B$ and $(3d_{yz})_{AB}$ contribute to the next MOs with comparable energies, and $(3d_{xz})_{AB}$ is the highest complex MO with significant metal $3d$ contributions. One-electron calculations of the Wolfsberg–Helmholtz type on **1a**/**2a** and **1c**/**2c** respectively predicted this MO sequence [47].

A schematical representation of the ordering of complex MOs with large metal $3d$ contributions is shown in Fig. 3.

In the Fe derivatives **1a** and **2a** only the six lowest $3d$ combinations are occupied. Two additional electrons in $(3d_{xz})_B$ corresponds to the ground state configuration of the Co complexes **1b** and **2b**. In the Ni dimers **1c** and **2c** four electrons occupy

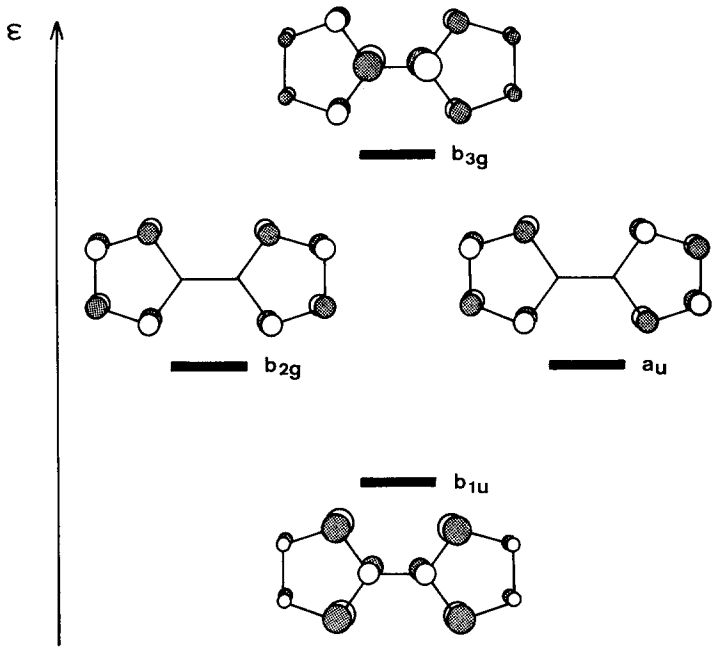

Fig. 2. Schematical representation and ordering of the π^* acceptor orbitals of the fulvalene dianion according to the HMO model

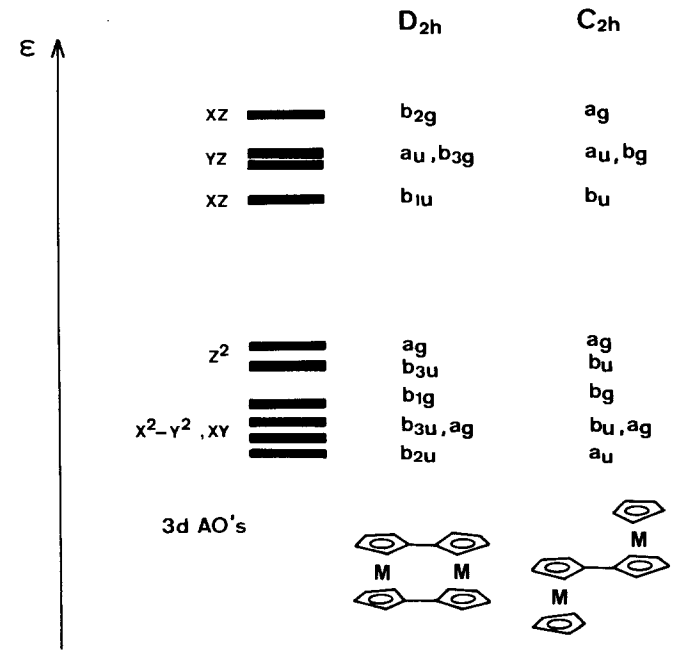

Fig. 3. Energy ordering of the binuclear complex MOs with large metal $3d$ contributions in the bimetallocene and bimetallocenylene series **1** and **2** on the basis of one-electron arguments

the high lying $3d$ linear combinations with large $3d_{xz}/3d_{yz}$ amplitudes. In the Cr bisfulvalene, **2d**, only the four MOs associated with the $3d_{x2-y2}$ and $3d_{xy}$ AOs are occupied, while the $3d_{z2}$ MO set belongs to the particle functions. A detailed description of the electronic structure of **1a** and **2a** is given in Ref. 27 and 47.

Table 1. Results of the singlet instabilities of **1a** according to the INDO method; the orbital fluctuations, their contribution to the roots, the MO-type of the hole- and particle-states as well as the metal $3d$ contribution to the corresponding orbitals is also given

i	λ_i (eV)	$\phi_k \rightarrow \phi_l$	%	MO-Type ϕ_k	MO-Type ϕ_l	% $3d\,\phi_k$	% $3d\,\phi_l$
1	1.14	$(17a_g) \rightarrow (14a_u)$	49.6	$(3d_{z2})_B$	$(3d_{yz})_{AB}, L(\pi^*)$	91.2	59.9
		$(16b_u) \rightarrow (14b_g)$	45.7	$(3d_{z2})_{AB}$	$(3d_{yz})_B, L(\pi^*)$	86.7	59.2
2	1.14	$(17a_g) \rightarrow (14b_g)$	49.5		see $i = 1$		
		$(16b_u) \rightarrow (14a_u)$	45.8				
3	1.71	$(15a_g) \rightarrow (14b_g)$	48.0	$(3d_{x2-y2})_B$	$(3d_{yz})_B, L(\pi^*)$	89.1	59.2
		$(15b_u) \rightarrow (14a_u)$	30.3	$(3d_{x2-y2})_{AB}, L(\pi)$	$(3d_{yz})_{AB}, L(\pi^*)$	62.4	59.9
		$(14b_u) \rightarrow (14a_u)$	17.8	$(3d_{x2-y2})_{AB}, L(\pi)$	$(3d_{yz})_{AB}, L(\pi^*)$	45.6	59.9
4	1.71	$(15a_g) \rightarrow (14a_u)$	48.2				
		$(15b_u) \rightarrow (14b_g)$	30.3		see $i = 3$		
		$(14b_u) \rightarrow (14b_g)$	17.8				
5	1.73	$(9a_g) \rightarrow (14a_u)$	49.6	$(3d_{xy})_{AB}$	$(3d_{yz})_{AB}, L(\pi^*)$	89.1	59.9
		$(9a_u) \rightarrow (14b_g)$	49.6	$(3d_{xy})_B$	$(3d_{yz})_B, L(\pi^*)$	91.9	59.2
6	1.73	$(9a_u) \rightarrow (14a_u)$	49.7		see $i = 5$		
		$(9b_g) \rightarrow (14b_g)$	49.6				
7	2.15	$(16b_u) \rightarrow (20a_u)$	46.4	$(3d_{z2})_{AB}$	$(3d_{xz})_B, L(\pi^*)$	86.9	49.6
		$(17a_g) \rightarrow (20a_g)$	32.6	$(3d_{z2})_B$	$L(\pi^*), (3d_{xz})_{AB}$	91.2	23.7
		$(17a_g) \rightarrow (19a_g)$	15.1	$(3d_{z2})_B$	$L(\pi^*), (3d_{xz})_{AB}$	91.2	18.6
8	2.15	$(17a_g) \rightarrow (20a_u)$	50.4				
		$(16b_u) \rightarrow (20a_g)$	29.9		see $i = 7$		
		$(16b_u) \rightarrow (19a_g)$	14.3				
9	2.71	$(15a_g) \rightarrow (20a_u)$	46.1	$(3d_{x2-y2})_B$	$(3d_{xz})_B, L(\pi^*)$	89.1	49.6
		$(15b_u) \rightarrow (20a_g)$	19.5	$(3d_{x2-y2})_{AB}, L(\pi)$	$L(\pi^*), (3d_{xz})_{AB}$	62.4	23.7
		$(14b_u) \rightarrow (20a_g)$	9.9	$(3d_{x2-y2})_{AB}, L(\pi)$	$L(\pi^*), (3d_{xz})_{AB}$	45.6	23.7
		$(15b_u) \rightarrow (19a_g)$	8.9	$(3d_{x2-y2})_{AB}, L(\pi)$	$L(\pi^*), (3d_{xz})_{AB}$	62.4	18.6
10	2.73	$(9a_u) \rightarrow (20a_u)$	50.6	$(3d_{xy})_B$	$(3d_{xz})_B, L(\pi^*)$	91.1	49.6
		$(9b_g) \rightarrow (20a_g)$	32.8	$(3d_{xy})_{AB}$	$L(\pi^*), (3d_{xz})_{AB}$	89.1	23.7
		$(9b_g) \rightarrow (19a_g)$	15.4	$(3d_{xy})_{AB}$	$L(\pi^*), (3d_{xz})_{AB}$	89.1	18.6
11	2.75	$(9b_g) \rightarrow (20a_u)$	50.8				
		$(9a_u) \rightarrow (20a_g)$	32.8		see $i = 11$		
		$(9a_u) \rightarrow (19a_g)$	15.3				
12	2.78	$(15a_g) \rightarrow (20a_g)$	30.5	$(3d_{x2-y2})_B$	$L(\pi^*), (3d_{xz})_{AB}$	89.1	23.7
		$(14b_u) \rightarrow (20a_u)$	28.9	$(3d_{x2-y2})_{AB}, L(\pi)$	$(3d_{xz})_B, L(\pi^*)$	45.6	49.6
		$(15a_g) \rightarrow (19a_g)$	18.4	$(3d_{x2-y2})_B$	$L(\pi^*), (3d_{xz})_{AB}$	89.1	18.6
		$(15b_u) \rightarrow (20a_u)$	15.0	$(3d_{x2-y2})_{AB}, L(\pi)$	$(3d_{xz})_B, L(\pi^*)$	62.4	49.6

Table 2. Results of the singlet instabilities of **2a** according to the INDO method. Legend see Table 1

i	λ_i (eV)	$\phi_k \rightarrow \phi_l$	%	MO-Type ϕ_k	MO-Type ϕ_l	% $3d\ \phi_k$	% $3d\ \phi_l$
1	1.22	$(8b_{3u}) \rightarrow (7b_{3g})$	48.6	$(3d_{z2})_{AB}$	$(3d_{yz})_B$, $L(\pi^*)$	90.3	58.0
		$(10a_g) \rightarrow (7b_{3g})$	28.8	$L(\pi)$, $(3d_{z2})_B$	$(3d_{yz})_B$, $L(\pi^*)$	52.9	58.0
		$(9a_g) \rightarrow (7a_u)$	19.4	$(3d_{z2})_B$, $L(\pi)$	$(3d_{yz})_{AB}$, $L(\pi^*)$	59.2	57.8
2	1.23	$(8b_{3u}) \rightarrow (7a_u)$	48.3				
		$(10a_g) \rightarrow (7b_{3g})$	29.1		see $i = 1$		
		$(9a_g) \rightarrow (7b_{3g})$	19.1				
3	1.46	$(10a_g) \rightarrow (10b_{1u})$	25.6	$L(\pi)$, $(3d_{z2})_B$	$(3d_{xz})_B$, $L(\pi^*)$	52.9	53.2
		$(8b_{3u}) \rightarrow (10b_{2g})$	22.5	$(3d_{z2})_{AB}$	$L(\pi^*)$, $(3d_{xz})_{AB}$	90.3	27.7
		$(9a_g) \rightarrow (10b_{1u})$	20.9	$(3d_{z2})_B$, $L(\pi)$	$(3d_{xz})_B$, $L(\pi^*)$	59.2	53.2
		$(8b_{3u}) \rightarrow (9b_{2g})$	19.2	$(3d_{z2})_{AB}$	$L(\pi^*)$, $(3d_{xz})_{AB}$	90.3	21.1
4	1.47	$(8b_{3u}) \rightarrow (10b_{1u})$	45.2				
		$(10a_g) \rightarrow (10b_{2g})$	13.2		see $i = 3$		
		$(10a_g) \rightarrow (9b_{2g})$	11.0				
		$(9a_g) \rightarrow (10b_{2g})$	9.8				
5	1.67	$(7b_{3u}) \rightarrow (7b_{3g})$	48.0	$(3d_{x2-y2})_{AB}$	$(3d_{yz})_B$, $L(\pi^*)$	89.5	58.0
		$(8a_g) \rightarrow (7a_u)$	33.8	$(3d_{x2-y2})_B$, $L(\pi)$	$(3d_{yz})_{AB}$, $L(\pi^*)$	70.6	57.8
		$(9a_g) \rightarrow (7a_u)$	11.5	$(3d_{z2})_B$, $L(\pi)$	$(3d_{yz})_{AB}$, $L(\pi^*)$	59.2	57.8
6	1.68	$(7b_{3u}) \rightarrow (7a_u)$	48.1				
		$(8a_g) \rightarrow (7b_{3g})$	33.9		see $i = 5$		
		$(9a_g) \rightarrow (7b_{3g})$	12.1				
7	1.80	$(7b_{3u}) \rightarrow (10b_{1u})$	29.3	$(3d_{x2-y2})_{AB}$	$(3d_{xz})_B$, $L(\pi^*)$	89.5	53.2
		$(5b_{2u}) \rightarrow (7a_u)$	13.6	$(3d_{xy})_B$	$(3d_{yz})_{AB}$, $L(\pi^*)$	91.0	57.8
		$(5b_{1g}) \rightarrow (7b_{3g})$	13.6	$(3d_{xy})_{AB}$	$(3d_{yz})_B$, $L(\pi^*)$	84.2	58.0
		$(8a_g) \rightarrow (10b_{2g})$	12.0	$(3d_{x2-y2})_B$, $L(\pi)$	$L(\pi^*)$, $(3d_{xz})_{AB}$	70.6	27.7
8	1.85	$(5b_{2u}) \rightarrow (7b_{3g})$	49.4	$(3d_{xy})_B$	$(3d_{yz})_B$, $L(\pi^*)$	84.2	58.0
		$(5b_{1g}) \rightarrow (7a_u)$	48.8	$(3d_{xy})_{AB}$	$(3d_{yz})_{AB}$, $L(\pi^*)$	91.0	57.8
9	1.87	$(5b_{2u}) \rightarrow (7a_u)$	35.7	$(3d_{xy})_B$	$(3d_{yz})_{AB}$, $L(\pi^*)$	84.2	57.8
		$(5b_{1g}) \rightarrow (7b_{3g})$	35.7	$(3d_{xy})_{AB}$	$(3d_{yz})_B$, $L(\pi^*)$	91.0	58.0
		$(7b_{3u}) \rightarrow (10b_{1u})$	11.6	$(3d_{x2-y2})_{AB}$	$(3d_{xz})_B$, $L(\pi^*)$	89.5	53.2
10	2.00	$(8a_g) \rightarrow (10b_{1u})$	33.1	$(3d_{x2-y2})_B$, $L(\pi)$	$(3d_{xz})_B$, $L(\pi^*)$	70.6	53.2
		$(7b_{3u}) \rightarrow (10b_{2g})$	22.1	$(3d_{x2-y2})_{AB}$	$L(\pi^*)$, $(3d_{xz})_{AB}$	89.5	27.7
		$(7b_{3u}) \rightarrow (9b_{2g})$	20.7	$(3d_{x2-y2})_{AB}$	$L(\pi^*)$, $(3d_{xz})_{AB}$	89.5	21.1
		$(9a_g) \rightarrow (10b_{1u})$	9.6	$(3d_{z2})_B$, $L(\pi)$	$(3d_{xz})_B$, $L(\pi^*)$	59.2	53.2
11	2.08	$(5b_{1g}) \rightarrow (10b_{1u})$	46.1	$(3d_{xy})_{AB}$	$(3d_{xz})_B$, $L(\pi^*)$	91.0	53.2
		$(5b_{2u}) \rightarrow (10b_{2g})$	23.4	$(3d_{xy})_B$	$L(\pi^*)$, $(3d_{xz})_{AB}$	84.2	27.2
		$(5b_{2u}) \rightarrow (9b_{2g})$	19.6	$(3d_{xy})_B$	$L(\pi^*)$, $(3d_{xz})_{AB}$	84.2	21.1
		$(5b_{1g}) \rightarrow (9b_{1u})$	9.5	$(3d_{xy})_{AB}$	$L(\pi^*)$, $(3d_{xz})_B$	91.0	7.4
12	2.10	$(5b_{2u}) \rightarrow (10b_{1u})$	47.1				
		$(5b_{1g}) \rightarrow (10b_{2g})$	23.4		see $i = 11$		
		$(5b_{1g}) \rightarrow (9b_{2g})$	19.6				
		$(5b_{2u}) \rightarrow (9b_{1u})$	9.5				

Table 3. Comparison of the roots of the singlet, non-singlet and non-real variations in **2a** and **1a** according to the INDO method; all values in eV.

λ_i	**2a**			**1a**		
i	$^1\lambda_i$	$^3\lambda_i$	$^c\lambda_i$	$^1\lambda_i$	$^3\lambda_i$	$^c\lambda_i$
1	1.22	1.19	1.21	1.14	1.10	1.12
2	1.23	1.19	1.22	1.14	1.10	1.12
3	1.46	1.40	1.45	1.71	1.62	1.68
4	1.47	1.42	1.46	1.71	1.62	1.69
5	1.67	1.42	1.63	1.73	1.68	1.71
6	1.68	1.44	1.63	1.73	1.68	1.71
7	1.80	1.54	1.83	2.15	2.12	2.14
8	1.85	1.75	1.83	2.15	2.12	2.14
9	1.87	1.80	1.88	2.71	2.37	2.71
10	2.00	1.81	1.93	2.73	2.50	2.73
11	2.08	2.05	2.07	2.75	2.65	2.74
12	2.10	2.07	2.09	2.78	2.68	2.74

5. HF Instabilities in the Fe Derivatives

The HF SCF ground state results based on the INDO Hamiltonian for **1a** and **2a** have been discussed previously [27]. The results of the singlet instabilities are summarized in Tables 1 (**1a**) and 2 (**2a**). The twelve lowest eigenvalues of the singlet fluctuations are given. It is seen that none of the roots is less than zero, so the HF picture represents a sufficient approximation to the exact ground state of **1a** and **2a**. The eigenvalues collected in Tables 1 and 2 correspond to the possible orbital transitions from the $3d_{z2}$, $3d_{x2-y2}$, and $3d_{xy}$ hole-states into the $3d_{xz}/3_{yz}$ particle-set. The absolute values of the roots indicate a variation of the importance of electron correlation within the various $3d$ linear combinations. The four lowest roots in **2a** correspond to orbital fluctuations out of $3d_{z2}$ MOs indicating the most pronounced correlation effects for these $3d$ functions. The remaining roots are associated with the $3d_{x2-y2}$ and $3d_{xy}$ MOs. In the biferrocene complex this separation between the different $3d$ fluctuations is reduced. Here only two excitations from $3d_{z2}$ linear combinations into $3d_{yz}$ particle-states are energetically separated. The twelve lowest roots of the non-singlet and non-real variations are collected in Table 3 and are compared with the singlet fluctuations. The three types of HF excitations in **1a** and **2a** are similar, and the eigenvalues and the contributions to the orbital transitions of the triplet and non-real route are close to the singlet instability. This result is expected for a dimeric species where the bonding and antibonding linear combinations of a definite $3d$ AO are always occupied.

6. HF Instabilities in the Co Derivatives

Four different SCF calculations were performed for each of the two Co compounds **1b** and **2b**. The four possible linear combinations of $3d_{xz}$ and $3d_{yz}$ (bonding and antibonding) were occupied with two electrons of opposite spin

(α, β) leading to a diamagnetic closed shell determinant. The relative energies of the four choices, the atomic populations and net charges [48] for **1b** and **2b** are collected in Tables 4 and 5. In both complexes the in-phase linear combination of the $3d_{xz}$ AOs leads to the SCF ground state; this result is in line with the qualitative expectations discussed in section 4. In bicobaltocene **1b** the determinant with $(3d_{xz})_B$ is separated by 87.71 kJ/mol from the MO wave function

Table 4. Co population, net charges and relative energies of the four possible RHF SCF states of **1b** according to the INDO method

Occupation	$(3d_{xz})_B$	$(3d_{yz})_{AB}$	$(3d_{yz})_B$	$(3d_{xz})_{AB}$
ΔE (kJ/mol)	0.00	87.71	90.04	106.57
Co 4*s*	0.0656	0.0656	0.0656	0.0657
$4p_x$	0.0309	0.0310	0.0310	0.0310
$4p_y$	0.0284	0.0284	0.0284	0.0285
$4p_z$	0.0507	0.0507	0.0507	0.0507
$3d_{z2}$	1.9957	1.9966	1.9966	1.9965
$3d_{xz}$	1.6565	0.7026	0.7032	1.6113
$3d_{yz}$	0.6883	1.6267	1.6271	0.7067
$3d_{x2-y2}$	1.9404	1.9455	1.9452	1.9460
$3d_{xy}$	1.9426	1.9455	1.9444	1.9457
Net charges Co	0.6009	0.6085	0.6078	0.6179
C_1=C_4	−0.2103	−0.2345	−0.2306	−0.2355
C_2=C_3	−0.1548	−0.1837	−0.1829	−0.2005
C_{10}	−0.0725	−0.0379	−0.0414	−0.0363
C_{11}=C_{14}	−0.1818	−0.2101	−0.2113	−0.1878
C_{12}=C_{13}	−0.2246	−0.1943	−0.1956	−0.1972
C_{15}	−0.2242	−0.1752	−0.1746	−0.1934

Table 5. Co population, net charges and relative energies of the four possible RHF SCF states of **2b** according to the INDO method

Occupation	$(3d_{xz})_B$	$(3d_{yz})_B$	$(3d_{yz})_{AB}$	$(3d_{xz})_{AB}$
ΔE (kJ/mol)	0.00	107.20	113.09	161.37
Co 4*s*	0.0657	0.0658	0.0658	0.0660
$4p_x$	0.0336	0.0338	0.0338	0.0338
$4p_y$	0.0288	0.0288	0.0288	0.0290
$4p_z$	0.0514	0.0514	0.0514	0.0515
$3d_{z2}$	1.9963	1.9964	1.9964	1.9965
$3d_{xz}$	1.7073	0·7207	0·7217	1·5569
$3d_{yz}$	0.6519	1.6214	1.6186	0·7583
$3d_{x2-y2}$	1.9458	1.9474	1.9478	1.9495
$3d_{xy}$	1.9439	1.9457	1.9458	1.9487
Net charges Co	0.5752	0.5887	0.5898	0.6099
C_1=C_4	−0.1965	−0.2332	−0.2334	−0.2229
C_2=C_3	−0.1893	−0.1806	−0.1809	−0.1942
C_{10}	−0.0715	−0.0296	−0.0295	−0.0356

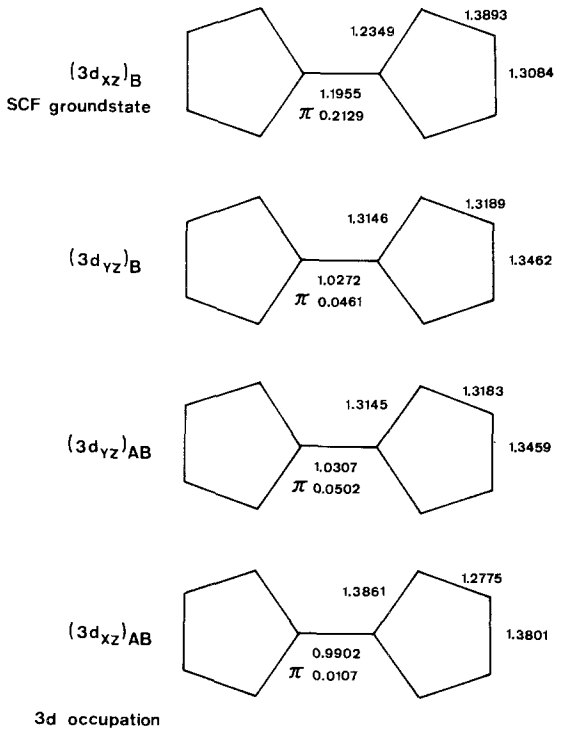

Fig. 4. Wiberg bond indices of the four SCF states of **2b**. In the case of the central CC-bond the π-contribution to the net index is given separately

with the out-of-phase combination of $3d_{yz}$; the near degeneracy between $(3d_{yz})_{AB}$ and $(3d_{yz})_B$ is seen in Table 4 ($\Delta E = 2.34$ kJ/mol). $(3d_{xz})_{AB}$ is separated by 106.57 kJ/mol from the SCF ground state. The same energy pattern is encountered in the bisfulvalene derivative **2b**. The energy width of the four SCF solutions however is greater in **2b** than in **1b**. The $3d_{z2}$, $3d_{x2-y2}$ and $3d_{xy}$ orbitals always have atomic populations that exceed 1.90 e. The atomic population of the "occupied" high lying Co $3d$ set lies between 1.55 and 1.70 e, while the second AO within the $3d_{xz}/3d_{yz}$ family is populated by about 0.7 e. Tables 4 and 5 also indicate that the differences within the Co $3d$ population create significant charge drifts in the organic π-systems.

A sensitive probe for the charge reorganization in the organic ligands due to different $3d$ AO populations consists in the Wiberg bond indices [49] in the fulvalene fragment. In Fig. 4 the bond indices in the $C_{10}H_8$ moiety of **2b** are collected. It is seen that only $(3d_{xz})_B$ leads to a perceptible π-coupling between the formal cp fragments (π contribution 0.2129 between C_9 and C_{10}). Of course the π interaction goes to zero in the $(3d_{xz})_{AB}$ occupation pattern. $(3d_{xz})_{AB}$ also leads to a charge accumulation between the terminal carbon centers of the cp rings. The gradual change in the π density alternation can be rationalized on the basis of Fig. 2.

In Tables 6 and 7 we have collected the results of the HF singlet fluctuations obtained for **1b** and **2b**; in both systems the eight lowest roots are collected.

Table 6. Results of the singlet instabilities of **1b** according to the INDO method; legend see Table 1

i	λ_i (eV)	$\phi_k \rightarrow \phi_l$	%	MO-Type ϕ_k	MO-Type ϕ_l	% $3d\,\phi_k$	% $3d\,\phi_l$
1	0.09	$(18b_u) \rightarrow (14b_g)$	64.5	$L(\pi)$, $(3d_{xz})_B$	$(3d_{yz})_B$, $L(\pi^*)$	29.5	61.5
		$(18a_g) \rightarrow (13a_u)$	7.0	$L(\pi)$	$(3d_{yz})_{AB}$, $L(\pi^*)$	4.8	58.5
		$(16a_g) \rightarrow (13a_u)$	6.0	$(3d_{xz})_{AB}$, $L(\pi)$	$(3d_{yz})_{AB}$, $L(\pi^*)$	47.4	58.5
		$(14b_u) \rightarrow (14b_g)$	5.7	$(3d_{x2-y2})_{AB}$, $L(\pi)$	$(3d_{yz})_B$, $L(\pi^*)$	52.0	61.5
2	0.18	$(18b_u) \rightarrow (13a_u)$	61.8		see $i = 1$		
		$(18a_g) \rightarrow (14b_g)$	7.7				
		$(18b_u) \rightarrow (12a_u)$	6.7	$L(\pi)$, $(3d_{xz})_B$	$L(\pi^*)$, $(3d_{yz})_{AB}$	29.5	8.3
		$(16a_g) \rightarrow (14b_g)$	6.0		see $i = 1$		
		$(14b_u) \rightarrow (13a_u)$	5.8				
3	0.25	$(16b_u) \rightarrow (14b_g)$	43.3	$(3d_{z2})_{AB}$	$(3d_{yz})_B$, $L(\pi^*)$	90.8	61.5
		$(17a_g) \rightarrow (13a_u)$	41.4	$(3d_{z2})_B$	$(3d_{yz})_{AB}$, $L(\pi^*)$	90.2	58.5
4	0.25	$(17a_g) \rightarrow (14b_g)$	42.9		see $i = 3$		
		$(16b_u) \rightarrow (13a_u)$	40.6				
5	0.50	$(9a_u) \rightarrow (14b_g)$	47.1	$(3d_{xy})_B$	$(3d_{yz})_B$, $L(\pi^*)$	95.1	61.5
		$(9b_g) \rightarrow (13a_u)$	44.4	$(3d_{xy})_{AB}$	$(3d_{yz})_{AB}$, $L(\pi^*)$	92.2	58.5
6	0.50	$(9b_g) \rightarrow (14b_g)$	46.8		see $i = 5$		
		$(9a_u) \rightarrow (13a_u)$	44.8				
7	0.58	$(15a_g) \rightarrow (13a_u)$	34.3	$(3d_{x2-y2})_B$	$(3d_{yz})_{AB}$, $L(\pi^*)$	88.8	58.5
		$(15b_u) \rightarrow (14b_g)$	30.7	$(3d_{x2-y2})_{AB}$, $L(\pi)$	$(3d_{yz})_B$, $L(\pi^*)$	69.5	61.5
		$(14b_u) \rightarrow (14b_g)$	12.4	$(3d_{x2-y2})_{AB}$, $L(\pi)$	$(3d_{yz})_B$, $L(\pi^*)$	52.0	61.5
8	0.60	$(15a_g) \rightarrow (14b_g)$	34.3				
		$(15b_u) \rightarrow (13a_u)$	29.3		see $i = 7$		
		$(14b_u) \rightarrow (13a_u)$	10.8				
		$(16a_g) \rightarrow (14b_g)$	7.6	$(3d_{xz})_{AB}$, $L(\pi)$	$(3d_{yz})_B$, $L(\pi^*)$	47.4	61.5

For reasons of clearness at first the bisfulvalene case **2b** with the higher symmetry is discussed. It is seen that always two roots are nearly degenerate (0.11/0.12 eV, 0.18/0.19 eV, 0.30/0.30 eV, 0.43/0.47 eV) and close to zero. Hence there are several singlet fluctuations leading to wave functions that are close to the energy of the HF determinant $|\phi_0\rangle$. Therefore it cannot be expected that the HF SCF solution contributes predominantly to the exact ground state.

The results in Table 7 indicate that the singlet fluctuations correspond to orbital excitations between electron-hole pairs with large $3d$ amplitudes; $3d_{yz}$ combinations in each correlation process are the particle MO. With respect to the $3d$ hole-states the following sequence of increasing correlation strength is encountered:

$$(3d_{xy}) < (3d_{x2-y2}) < (3d_{xz}) < (3d_{z2}).$$

A schematical representation of the orbital transitions $(8b_{3u}) \rightarrow (6b_{3g})$ and $(9a_g) \rightarrow (6a_u)$, which are the most important contributions to λ_1, is shown in Fig. 5.

Table 7. Results of the singlet instabilities of **2b** according to the INDO method; legend see Table 1

i	λ_i (eV)	$\phi_k \rightarrow \phi_l$	%	MO-Type ϕ_k	MO-Type ϕ_l	% $3d\,\phi_k$	% $3d\,\phi_l$
1	0.11	$(8b_{3u}) \rightarrow (6b_{3g})$	48.9	$(3d_{z2})_{AB}$	$(3d_{yz)B}$, $L(\pi^*)$	90.7	67.0
		$(9a_g) \rightarrow (6a_u)$	38.1	$(3d_{z2})_B$	$(3d_{yz})_{AB}$, $L(\pi^*)$	84.4	66.3
		$(10a_g) \rightarrow (6a_u)$	9.3	$L(\pi)$, $(3d_z2)_B$	$(3d_{yz})_{AB}$, $L(\pi^*)$	19.5	66.3
2	0.12	$(8b_{3u}) \rightarrow (6a_u)$	48.6				
		$(9a_g) \rightarrow (6b_{3g})$	38.0		see $i = 1$		
		$(10a_g) \rightarrow (6b_{3g})$	9.6				
3	0.18	$(9b_{1u}) \rightarrow (6a_u)$	73.9	$L(\pi)$, $(3d_{xz})_B$	$(3d_{yz})_{AB}$, $L(\pi^*)$	35.8	66.3
		$(7b_{2g}) \rightarrow (6b_{3g})$	12.6	$L(\pi)$, $(3d_{xz})_{AB}$	$(3d_{yz})_B$, $L(\pi^*)$	44.6	67.0
4	0.19	$(9b_{1u}) \rightarrow (6b_{3g})$	75.5		see $i = 3$		
		$(7b_{2g}) \rightarrow (6a_u)$	12.2				
5	0.30	$(7b_{3u}) \rightarrow (6b_{3g})$	49.5	$(3d_{x2-y2})_{AB}$	$(3d_{yz})_B$, $L(\pi^*)$	94.2	67.0
		$(8a_g) \rightarrow (6a_u)$	40.0	$(3d_{x2-y2})_B$	$(3d_{yz})_{AB}$, $L(\pi^*)$	84.9	66.3
6	0.30	$(7b_{3u}) \rightarrow (6a_u)$	48.9		see $i = 5$		
		$(8a_g) \rightarrow (6b_{3g})$	40.2				
7	0.43	$(5b_{2u}) \rightarrow (6b_{3g})$	40.0	$(3d_{xy})_B$	$(3d_{yz})_B$, $L(\pi^*)$	96.0	67.0
		$(5b_{1g}) \rightarrow (6a_u)$	38.5	$(3d_{xy})_{AB}$	$(3d_{yz})_{AB}$, $L(\pi^*)$	88.0	66.3
		$(9b_{1u}) \rightarrow (11a_g)$	9.7	$L(\pi)$, $(3d_{xz})_B$	$L(\pi^*)$, $(3d_{x2-y2})_B$	35.8	3.1
8	0.47	$(5b_{2u}) \rightarrow (6a_u)$	49.8		see $i = 7$		
		$(5b_{1g}) \rightarrow (6b_{3g})$	48.9				

It is clearly seen that the correlation type in the various singlet fluctuations corresponds to an angular many-body interaction between $3d$ orbitals of different z components of the magnetic quantum numbers. This result has also been verified in the study of Kanamori on correlation effects in band-structures of

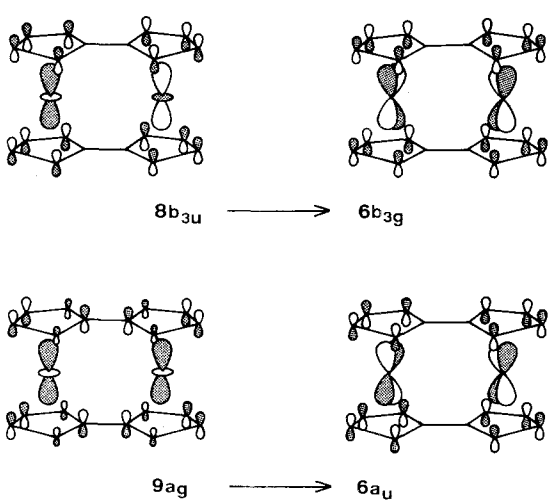

Fig. 5. Schematical representation of the MOs $8b_{3u}$, $6b_{3g}$, $9a_g$ and $6a_u$ contributing predominantly to the first root of the singlet instability for **2b**

transition metals [50]. In the case of MOs with different parity (g/u, i/o symmetry) the angular correlation is formally coupled to an interatomic left–right correlation. Our recent investigation on poly-decker sandwich compounds has demonstrated that both many-body mechanisms contributed with comparable magnitudes to the net singlet fluctuation. The degeneracy between g/u pairs on one side and that between u/u or g/g excitations on the other side, however, indicate, that left–right correlation in **2b** is without any significance in the singlet instability problem.

This different behaviour in the two kinds of polynuclear complexes (bimetallocenes, poly-decker sandwiches) with respect to both correlation types (angular,

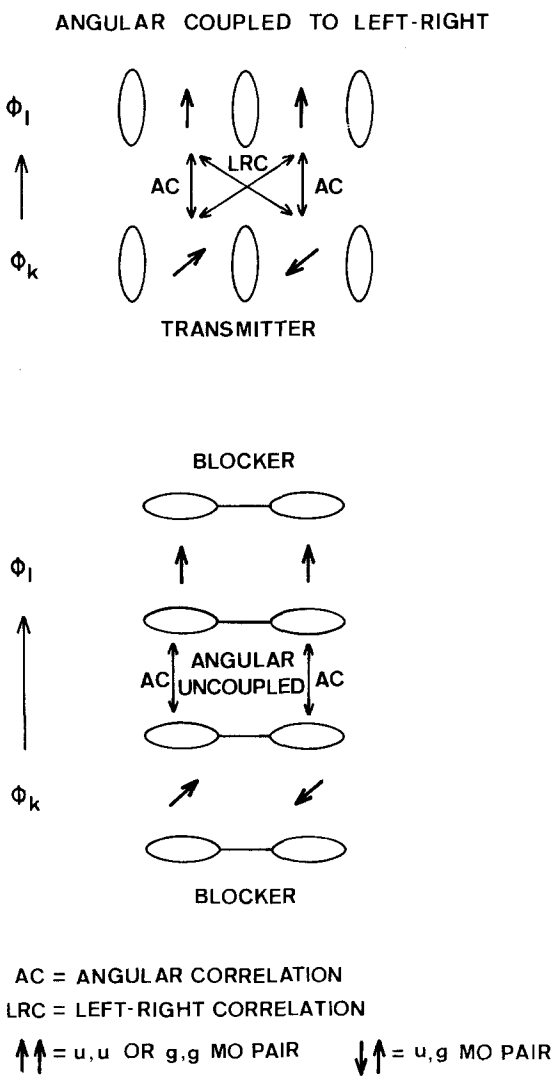

Fig. 6. Differences for the singlet fluctuations in triple-decker sandwiches (top) and bimetallocenes (bottom). Coupling of angular and left–right correlation in the stacked sandwiches, localized angular fluctuations in the bridged sandwiches

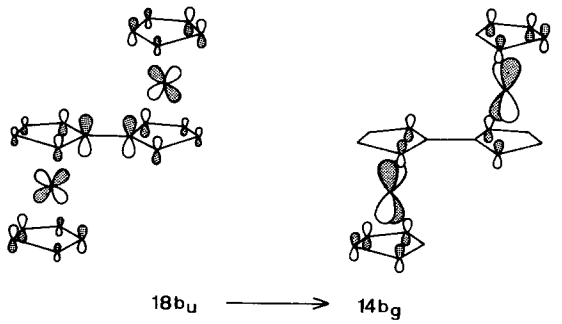

Fig. 7. Schematical representation of the electron-hole pair $18b_u/14b_g$ leading to the lowest root of the singlet instability in **1b**

left–right) can be explained by means of the schematical drawings in Fig. 5. It is seen that the MOs with large $3d_{yz}$ contributions (particle-states for the HF-fluctuations) have a node at the terminal CC-bond due to the symmetry of $3d_{yz}$. Therefore the coupling between both fragments is very weak and long-range

Table 8. Results of the non-singlet (triplet) instabilities of **1b** according to the INDO method; legend see Table 1

i	λ_i (eV)	$\phi_k \rightarrow \phi_l$	%	MO-Type ϕ_k	MO-Type ϕ_l	% $3d\,\phi_k$	% $3d\,\phi_l$
1	−2.30	$(18b_u) \rightarrow (19a_g)$	87.7	$L(\pi)$, $(3d_{xz})_B$	$L(\pi^*)$, $(3d_{xz})_{AB}$	29.5	27.9
2	−0.04	$(18b_u) \rightarrow (13b_g)$	65.5	$L(\pi)$, $(3d_{xz})_B$	$(3d_{yz})_B$, $L(\pi^*)$	29.5	61.5
		$(18a_g) \rightarrow (13a_u)$	8.9	$L(\pi)$	$(3d_{yz})_{AB}$, $L(\pi^*)$	4.8	58.5
		$(16a_g) \rightarrow (13a_u)$	7.7	$(3d_{xz})_{AB}$, $L(\pi)$	$(3d_{yz})_{AB}$, $L(\pi^*)$	47.7	58.5
		$(10a_u) \rightarrow (19a_g)$	5.1	$L(\pi)$, $(3d_{yz})_{AB}$	$L(\pi^*)$, $(3d_{xz})_{AB}$	21.4	27.9
3	0.05	$(18b_u) \rightarrow (19b_u)$	69.9	$L(\pi)$, $(3d_{xz})_B$	$L(\pi^*)$, $(3d_{xz})_B$	29.5	8.7
		$(18a_g) \rightarrow (19a_g)$	14.9	$L(\pi)$	$L(\pi^*)$, $(3d_{xz})_{AB}$	4.8	58.5
		$(16a_g) \rightarrow (19a_g)$	9.5	$(3d_{xz})_{AB}$, $L(\pi)$	$L(\pi^*)$, $(3d_{xz})_{AB}$	47.4	58.5
4	0.07	$(18b_u) \rightarrow (13a_u)$	62.1				
		$(18a_g) \rightarrow (13b_g)$	9.3		see $i = 2$		
		$(16a_g) \rightarrow (13b_g)$	8.2				
5	0.19	$(16b_u) \rightarrow (13b_g)$	42.7	$(3d_{z2})_{AB}$	$(3d_{yz})_B$, $L(\pi^*)$	90.8	61.5
		$(17a_g) \rightarrow (13a_u)$	40.6	$(3d_{z2})_B$	$(3d_{yz})$, $L(\pi^*)$	90.2	58.5
6	0.20	$(17a_g) \rightarrow (13b_g)$	40.3		see $i = 5$		
		$(16b_u) \rightarrow (13a_u)$	38.3				
7	0.48	$(9a_u) \rightarrow (13b_g)$	46.9	$(3d_{xy})_B$	$(3d_{yz})_B$, $L(\pi^*)$	95.1	61.5
		$(9b_g) \rightarrow (13a_u)$	44.2	$(3d_{xy})_{AB}$	$(3d_{yz})_{AB}$, $L(\pi^*)$	92.2	58.5
8	0.48	$(9b_g) \rightarrow (13b_g)$	46.3		see $i = 7$		
		$(9a_u) \rightarrow (13a_u)$	44.2				
9	0.55	$(15a_g) \rightarrow (13a_u)$	35.5	$(3d_{x2-y2})_B$	$(3d_{yz})_{AB}$, $L(\pi^*)$	88.8	58.5
		$(15b_u) \rightarrow (13b_g)$	28.6	$(3d_{x2-y2})_{AB}$, $L(\pi)$	$(3d_{yz})_B$, $L(\pi^*)$	69.5	61.5
		$(14b_u) \rightarrow (13b_g)$	14.1	$(3d_{x2-y2})_{AB}$, $L(\pi)$	$(3d_{yz})_B$, $L(\pi^*)$	52.0	61.5
10	0.56	$(15a_g) \rightarrow (13g_g)$	35.7				
		$(15b_u) \rightarrow (13a_u)$	28.6		see $i = 9$		
		$(14b_u) \rightarrow (13a_u)$	14.1				

interactions cannot contribute to the singlet-variations. The many-body interaction retaining spin symmetry and violating spatial symmetry due to intraatomic angular correlation therefore is always associated with one metallocene fragment. The CC bridge acts as a "blocker" for the long-range contribution to the many-body interaction. In triple-decker sandwich compounds on the other hand the central ring system with π and σ MOs of different irreducible representations has the function of a "transmitter" between the $3d$ centers and allows an efficient coupling between the short-range angular and the long-range left–right correlation. Schematically these differences are displayed in Fig. 6.

The singlet fluctuations in the bimetallocene system **1b** are similar to the bisfulvalene case **2b** (Table 6). Once again degenerate eigenvalues in couples close to zero are predicted. In contrast to **2b** the HF fluctuation from $(3d_{xz})_B$ corresponds to the lowest roots, the remaining orbital excitations follow the pattern of **2b**. A schematical representation of the leading term of the orbital transitions of λ_1 is given in Fig. 7.

Table 9. Results of the non-singlet (triplet) instabilities of **2b** according to the INDO method; legend see Table 1

i	λ_i (eV)	$\phi_k \rightarrow \phi_l$	%	MO-Type ϕ_k	MO-Type ϕ_l	% $3d\,\phi_k$	% $3d\,\phi_l$
1	−1.97	$(9b_{1u}) \rightarrow (8b_{2g})$	95.9	$L(\pi)$, $(3d_{xz})_B$	$L(\pi^*)$, $(3d_{xz})_{AB}$	35.8	26.2
2	−0.17	$(9b_{3u}) \rightarrow (8b_{2g})$	71.8	$L(\pi)$	$L(\pi^*)$, $(3d_{xy})_{AB}$	1.0	26.2
		$(9b_{1u}) \rightarrow (11a_g)$	23.7	$L(\pi)$, $(3d_{xz})_B$	$L(\pi^*)$, $(3d_{x2-y2})_B$	35.8	3.1
3	0.02	$(9b_{1u}) \rightarrow (6b_{3g})$	70.1	$L(\pi)$, $(3d_{xz})_B$	$(3d_{yz})_B$, $L(\pi^*)$	36.8	67.0
		$(7b_{2g}) \rightarrow (6a_u)$	13.3	$L(\pi)$, $(3d_{xz})_{AB}$	$(3d_{yz})_{AB}$, $L(\pi^*)$	44.6	66.3
		$(5a_u) \rightarrow (8b_{2g})$	7.1	$L(\pi)$, $(3d_{yz})_{AB}$	$L(\pi^*)$, $(3d_{xz})_{AB}$	24.4	26.2
4	0.03	$(9b_{1u}) \rightarrow (6a_u)$	69.0	$L(\pi)$, $(3d_{xz})_B$	$(3d_{yz})_{AB}$, $L(\pi^*)$	35.8	66.3
		$(7b_{2g}) \rightarrow (6b_{3g})$	13.7	$L(\pi)$, $(3d_{xz})_{AB}$	$(3d_{yz})_B$, $L(\pi^*)$	44.6	67.0
		$(5b_{3g}) \rightarrow (8b_{2g})$	7.3	$L(\pi)$, $(3d_{yz})_B$	$L(\pi^*)$, $(3d_{xz})_{AB}$	25.8	26.2
5	0.08	$(8b_{3u}) \rightarrow (6a_u)$	47.3	$(3d_{z2})_{AB}$	$(3d_{yz})_{AB}$, $L(\pi^*)$	90.7	66.3
		$(9a_g) \rightarrow (6b_{3g})$	41.2	$(3d_{z2})_B$	$(3d_{yz})_B$, $L(\pi^*)$	84.4	67.0
		$(10a_g) \rightarrow (6b_{3g})$	8.2	$L(\pi)$, $(3d_{z2})_B$	$(3d_{yz})_B$, $L(\pi^*)$	19.5	67.0
6	0.08	$(8b_{3u}) \rightarrow (6b_{3g})$	47.9				
		$(9a_g) \rightarrow (6a_u)$	40.7		see $i = 5$		
		$(10a_g) \rightarrow (6a_u)$	8.2				
7	0.26	$(7b_{3u}) \rightarrow (6a_u)$	46.9	$(3d_{x2-y2})_{AB}$	$(3d_{yz})_{AB}$, $L(\pi^*)$	94.2	66.3
		$(8a_g) \rightarrow (6b_{3g})$	41.0	$(3d_{x2-y2})_B$	$(3d_{yz})_B$, $L(\pi^*)$	84.9	67.0
8	0.27	$(7b_{3u}) \rightarrow (6b_{3g})$	47.7		see $i = 7$		
		$(8a_g) \rightarrow (6a_u)$	40.6				
9	0.35	$(5b_{2u}) \rightarrow (6a_u)$	46.4	$(3d_{xy})_B$	$(3d_{yz})_{AB}$, $L(\pi^*)$	96.0	66.3
		$(5b_{1g}) \rightarrow (6b_{3g})$	45.4	$(3d_{xy})_{AB}$	$(3d_{yz})_B$, $L(\pi^*)$	88.0	67.0
10	0.36	$(5b_{2u}) \rightarrow (6b_{3g})$	47.6		see $i = 9$		
		$(5b_{1g}) \rightarrow (6a_u)$	45.5				

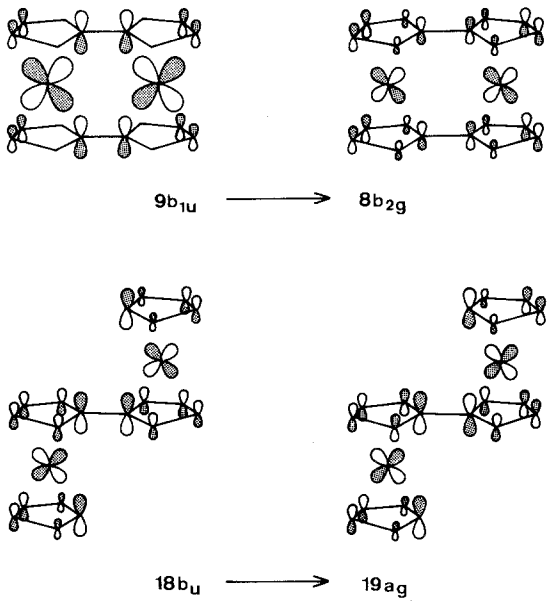

Fig. 8. Schematical representation of the electron-hole pair MOs in **1b** and **2b** leading to non-singlet instabilities

The results of the non-singlet (triplet) variations summarized in Tables 8 (**1b**) and 9 (**2b**) differ dramatically from the singlet instabilities. The lowest eigenvalue in both Co derivatives corresponds to a spin decoupling between an u/g MO pair with significant $3d_{xz}$ amplitudes. A figurative representation of the contributing MOs is displayed in Fig. 8.

The negative roots of the triplet variation indicate the existence of an UHF open shell determinant below the spin paired RHF solution. In both Co complexes the UHF solution predominantly profits from a single orbital transition (87.7% in **1b**, 95.9% in **2b**). The coupling to nearby correlation processes via the off-diagonal elements of the eigenvalue problem is of minor importance. The necessary condition for this spin decoupling (large exchange integrals in the diagonal elements of the instability matrix) has been mentioned in Sect. 2.

As the non-singlet fluctuation takes place between MOs with $3d_{xz}$ contributions, long-range effects between both monomer units are possible; they are transmitted due to the nonvanishing LCAO coefficients of the central bridge (see Fig. 8). This type of spin decoupling between two identical AOs at atomic sides with a large internuclear separation has been detected in various studies in the last thirty years [51, 52]. Generally this type of one-electron wave function violating spatial and spin symmetry is called an alternant molecular orbital (AMO) [53]; band-structure solutions that correspond to the molecular AMO case have also been discussed in the past [54].

The INDO results of the non-real instabilities obtained for **1b** and **2b** are collected in Table 10. The roots of Eq. (14) are compared with the eigenvalues of the singlet route. In analogy to the Fe complexes there is a close correspondence between both types of solutions.

Table 10. Comparison between the singlet and non-real eigenvalues in the Co derivatives **1b** and **2b**

	2b		**1b**	
i	$^1\lambda_i$ (eV)	$^c\lambda_i$ (eV)	$^1\lambda_i$ (eV)	$^c\lambda_i$ (eV)
1	0.11	0.10	0.09	0.05
2	0.12	0.10	0.18	0.15
3	0.18	0.14	0.25	0.22
4	0.19	0.16	0.25	0.23
5	0.30	0.30	0.50	0.49
6	0.30	0.30	0.50	0.49
7	0.43	0.45	0.58	0.57
8	0.47	0.45	0.60	0.58

7. HF Instabilities in the Ni Derivatives

In the case of the two Ni dimers **1c** and **2c** there are several possibilities to put four electrons with paired spins into the high lying $3d$ orbitals. The six practicable choices for the bisfulvalene system **2c** are compared in Table 11. The SCF ground state is that determinantal wave function where the bonding and antibonding linear combinations of $3d_{yz}$ are occupied. This filling scheme is separated from the corresponding $3d_{xz}$ occupation by only 13.12 kJ/mol. The other $3d$ configurations are significantly separated from the two lowest ones. $(3d_{xz})_B/(3d_{yz})_B$ is 223.14 kJ/mol above the SCF ground state, and $(3d_{xz})_{AB}/(3d_{yz})_{AB}$ is the highest one (406.98 kJ/mol above the SCF ground state).

In Table 12 relative SCF energies, Ni $3d$ populations and the atomic net charges of the binickelocene dimer **1c** are summarized. The calculated energy gap between the $(3d_{yz})_B/(3d_{yz})_{AB}$ ground state and the $3d_{xz}$ occupation pattern is 11.09 kJ/mol. In both Ni complexes four $3d$ AOs always show atomic populations near $2e$, $3d_{z2}$, $3d_{x2-y2}$, $3d_{xy}$ and one of the two high lying $3d$ functions ($3d_{xz}$ or $3d_{yz}$). The "unoccupied" $3d$ AO within $3d_{xz}/3d_{yz}$ is populated by about 1.10 e.

In Fig. 9 the Wiberg bond indices in the fulvalene moiety of **2c** are displayed for the SCF ground state and the $(3d_{xz})_B/(3d_{xz})_{AB}$ configuration. In both occupation patterns the π-coupling between the two cp rings is very small. It is seen that the two lowest SCF solutions correspond to two different VB structures for the fulvalene system. The SCF ground state contributes to the polyene structure I, the nearby state with occupied Ni $3d_{xz}$ AOs is associated with II where two ethylene fragments are formally coupled to a dimethylene-butenyl ribbon. Due

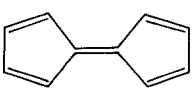

I

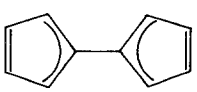

II

Table 11. Ni population, net charges and relative energies of the six possible symmetry adapted RHF SCF states of **2c** according to the INDO method. In the last column the results for the broken symmetry solution are summarized

Occupation	$(3d_{yz})_B$ $(3d_{yz})_{AB}$	$(3d_{xz})_B$ $(3d_{xz})_{AB}$	$(3d_{xz})_B$ $(3d_{yz})_B$	$(3d_{xz})_B$ $(3d_{yz})_{AB}$	$(3d_{xz})_{AB}$ $(3d_{yz})_B$	$(3d_{xz})_{AB}$ $(3d_{yz})_{AB}$	$(3d_{xz})_{loc}$ $(3d_{yz})_{loc}$	
ΔE (kJ/mol)	0.00	13.12	223.14	229.66	400.76	406.98	−4.34	
Ni $4s$	0.0452	0.0453	0.0453	0.0443	0.0446	0.0447	0.0452	0.0451
$4p_x$	0.0232	0.0229	0.0227	0.0227	0.0229	0.0229	0.0229	0.0231
$4p_y$	0.0197	0.0201	0.0196	0.0196	0.0197	0.0197	0.0201	0.0196
$4p_z$	0.0436	0.0437	0.0432	0.0432	0.0434	0.0434	0.0437	0.0436
$3d_{z2}$	1.9986	1.9986	1.9981	1.9981	1.9983	1.9983	1.9986	1.9985
$3d_{xz}$	1.0958	1.9979	1.7563	1.7596	1.5327	1.5204	1.9966	1.1277
$3d_{yz}$	1.9983	1.0881	1.5453	1.5380	1.6899	1.6970	1.0920	1.9982
$3d_{x2-y2}$	1.9838	1.9839	1.9735	1.9739	1.9779	1.9782	1.9842	1.9823
$3d_{xy}$	1.9832	1.9836	1.9727	1.9729	1.9774	1.9776	1.9835	1.9820
Net charges Ni	0.8086	0.8160	0.6244	0.6277	0.6930	0.6949	0.8131	0.7800
C_1=C_4	−0.3132	−0.1886	−0.2175	−0.2176	−0.2441	−0.2499	−0.1646	−0.3248
C_2=C_3	−0.1867	−0.2430	−0.1901	−0.1909	−0.1944	−0.1933	−0.2429	−0.1848
C_{10}	0.0089	−0.1148	−0.0561	−0.0563	−0.0371	−0.0341	−0.1561	0.0416

Table 12. Ni population, net charges and relative energies of the two lowest symmetry adapted RHF SCF states of **1c** according to the INDO method. In the last column the results for the broken symmetry solution are summarized

Occupation	$(3d_{yz})_B$ $(3d_{yz})_{AB}$	$(3d_{xz})_B$ $(3d_{xz})_{AB}$	$(3d_{xz})_{loc}$ $(3d_{yz})_{loc}$	
ΔE (kJ/mol)	0.00	11.09	4.16	
Ni 4*s*	0.0449	0.0450	0.0450	0.0449
$4p_x$	0.0213	0.0210	0.0210	0.0213
$4p_y$	0.0194	0.0198	0.0198	0.0194
$4p_z$	0.0430	0.0431	0.0431	0.0436
$3d_{z2}$	1.9986	1.9987	1.9987	1.9986
$3d_{xz}$	1.0757	1.9980	1.9979	1.0765
$3d_{yz}$	1.9982	1.0615	1.0653	1.9982
$3d_{x2-y2}$	1.9929	1.9837	1.9834	1.9829
$3d_{xy}$	1.9928	1.9833	1.9833	1.9827
Net charges Ni	0.8330	0.8460	0.8427	0.8323
C_1=C_4	−0.3151	−0.2100	−0.1882	−0.3347
C_2=C_{13}	−0.1967	−0.2493	−0.2485	−0.1929
C_{10}	−0.0069	−0.1147	−0.1608	−0.0382
C_{11}=C_{14}	−0.2937	−0.1449	−0.1407	−0.2938
C_{12}=C_{13}	−0.1965	−0.2521	−0.2513	−0.2005
C_{15}	−0.1142	−0.2973	−0.2971	−0.1220

to the near degeneracy of the two SCF solutions (I/II), it must be expected that the exact ground state is a superposition of both "VB structures". This result has been suggested also on the basis of experimental data obtained for **2c** [25].

In Tables 13 and 14 the lowest eigenvalues of the singlet, non-singlet and non-real variations of **1c** and **2c** are collected (SCF ground state). In the case

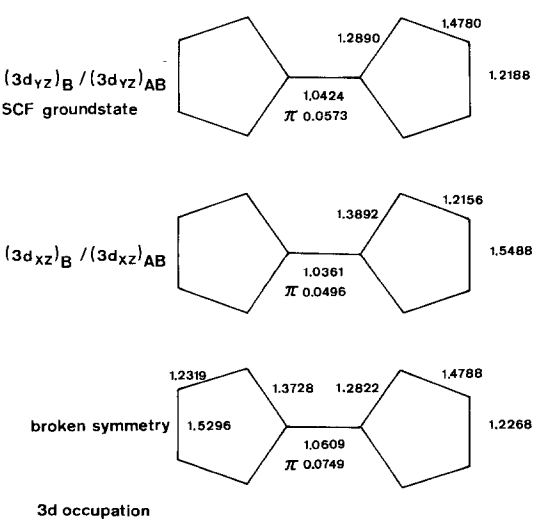

Fig. 9. Wiberg bond indices of the two lowest symmetry adapted SCF states of **2c**. Additionally the bond indices for the broken symmetry solution are given (bottom). In the case of the central CC-bond the π-contribution to the net index is given separately

Table 13. Results of the singlet, non-singlet and non-real instabilities of **1c** according to the INDO method; legend see Table 1

Type	i	λ_i (eV)	$\phi_k \rightarrow \phi_l$	%	MO-Type ϕ_k	MO-Type ϕ_l	% $3d\ \phi_k$	% $3d\ \phi_l$
Singlet	1	0.15	$(12a_u) \rightarrow (18b_u)$	50.8	$L(\pi)$, $(3d_{yz})_{AB}$	$(3d_{xz})_B$, $L(\pi^*)$	12.1	47.7
			$(12b_g) \rightarrow (19a_g)$	40.4	$L(\pi)$, $(3d_{yz})_B$	$(3d_{xz})_{AB}$, $L(\pi^*)$	12.4	43.3
	2	0.15	$(12b_g) \rightarrow (18b_u)$	51.5		see $i = 1$		
			$(12a_u) \rightarrow (19a_g)$	40.0				
Non-singlet	1	−1.47	$(17a_g) \rightarrow (19a_g)$	47.1	$(3d_{xz})_{AB}$, $L(\pi)$	$(3d_{xz})_{AB}$, $L(\pi^*)$	46.2	43.3
			$(16b_u) \rightarrow (18b_u)$	37.1	$L(\pi)$, $(3d_{xz})_B$	$(3d_{xz})_B$, $L(\pi^*)$	38.2	47.7
			$(17b_u) \rightarrow (18b_u)$	12.9	$L(\pi)$, $(3d_{xz})_B$	$(3d_{xz})_B$, $L(\pi^*)$	5.8	47.7
	2	−1.46	$(17a_g) \rightarrow (18b_u)$	55.2				
			$(16b_u) \rightarrow (19a_g)$	34.0		see $i = 1$		
			$(17b_u) \rightarrow (19a_g)$	8.4				
	3	−0.07	$(12a_u) \rightarrow (18b_u)$	48.0	$L(\pi)$, $(3d_{yz})_{AB}$	$(3d_{xz})_B$, $L(\pi^*)$	12.1	47.7
			$(12b_g) \rightarrow (19a_g)$	42.6	$L(\pi)$, $(3d_{yz})_B$	$(3d_{xz})_{AB}$, $L(\pi^*)$	12.4	43.3
	4	−0.07	$(12b_g) \rightarrow (18b_u)$	48.5		see $i = 3$		
			$(12a_u) \rightarrow (19a_g)$	42.6				
Non-real	1	0.07	$(12a_u) \rightarrow (18b_u)$	50.4		see $i = 1$ singlet		
			$(12b_g) \rightarrow (19a_g)$	41.5				
	2	0.07	$(12b_g) \rightarrow (18b_u)$	50.7		see $i = 1$		
			$(12a_u) \rightarrow (19a_g)$	41.4				

Table 14. Result of the singlet, non-singlet and non-real instabilities of **2c** according to the INDO method; legend see Table 1

Type	i	λ_i (eV)	$\phi_k \rightarrow \phi_l$	%	MO-Type ϕ_k	MO-Type ϕ_l	% $3d\ \phi_k$	% $3d\ \phi_l$
Singlet	1	0.09	$(6b_{3g}) \rightarrow (9b_{1u})$	60.4	$L(\pi)$, $(3d_{yz})_B$	$(3d_{xz})_B$, $L(\pi^*)$	12.1	50.8
			$(6a_u) \rightarrow (8b_{2g})$	31.8	$L(\pi)$, $(3d_{yz})_{AB}$	$(3d_{xz})_{AB}$, $L(\pi^*)$	11.8	38.1
	2	0.10	$(6a_u) \rightarrow (9b_{1u})$	61.4		see $i=1$		
			$(6b_{3g}) \rightarrow (8b_{2g})$	31.4				
Non-singlet	1	−1.47	$(7b_{2g}) \rightarrow (9b_{1u})$	72.3	$(3d_{xz})_{AB}$, $L(\pi)$	$(3d_{xz})_B$, $L(\pi^*)$	53.6	50.8
			$(8b_{1u}) \rightarrow (8b_{2g})$	26.9	$L(\pi)$, $(3d_{xz})_B$	$(3d_{xz})_{AB}$, $L(\pi^*)$	35.3	38.1
	2	−0.87	$(7b_{2g}) \rightarrow (8b_{2g})$	52.3		see $i=1$		
			$(8b_{1u}) \rightarrow (9b_{1u})$	46.6				
	3	−0.30	$(9b_{3u}) \rightarrow (9b_{1u})$	76.5	$L(\pi)$	$(3d_{xz})_B$, $L(\pi^*)$	0.2	50.8
			$(10a_g) \rightarrow (8b_{2g})$	16.4	$L(\pi)$	$(3d_{xz})_{AB}$, $L(\pi^*)$	0.8	38.1
	4	−0.12	$(6b_{3g}) \rightarrow (9b_{1u})$	54.2	$L(\pi)$, $(3d_{yz})_B$	$(3d_{xz})_B$, $L(\pi^*)$	12.1	50.8
			$(6a_u) \rightarrow (8b_{2g})$	37.1	$L(\pi)$, $(3d_{yz})_{AB}$	$(3d_{xz})_{AB}$, $L(\pi^*)$	11.8	38.1
	5	−0.11	$(6a_u) \rightarrow (9b_{1u})$	55.6		see $i=4$		
			$(6b_{3g}) \rightarrow (8b_{2g})$	36.2				
Non-real	1	0.02	$(6b_{3g}) \rightarrow (9b_{1u})$	58.3		see $i=1$		
			$(6a_u) \rightarrow (8b_{2g})$	34.3		singlet		
		0.03	$(6a_u) \rightarrow (8b_{2g})$	59.8		see $i=1$		
			$(6b_{3g}) \rightarrow (8b_{2g})$	35.5				

of the singlet fluctuations two degenerate eigenvalues near 0 are predicted indicating the strong influence of electron correlation upon the SCF ground state. A schematical representation of the orbital excitations is displayed in Figs. 10 and 11. It is seen that the HF fluctuations take place between occupied MOs with significant $3d_{yz}$ amplitudes and particle-states with predominant $3d_{xz}$ character. The important contributions to the many-body potential are therefore once

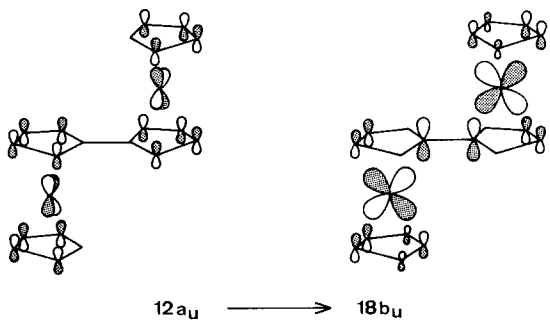

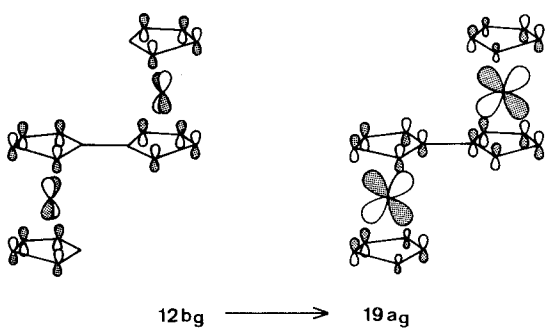

Fig. 10. Schematical representation of the MOs $12a_u$, $18b_u$, $12b_g$ and $19a_g$ contributing predominantly to the first root of the singlet instability for **1c**

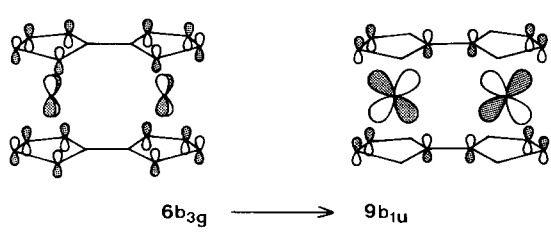

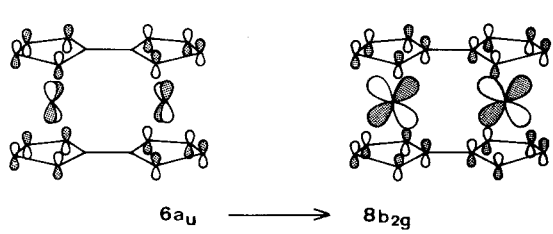

Fig. 11. Schematical representation of the MOs $6b_{3g}$, $9b_{1u}$, $6a_u$ and $8b_{2g}$ contributing predominantly to the first root of the singlet instability for **2c**

again intraatomic angular correlations at the $3d$ sides. This angular fluctuation enhances the electron density in $3d_{xz}$ and reduces the $3d_{yz}$ population. The degeneracy of the eigenvalues furthermore demonstrates the negligible contribution of the left–right correlation. The origin of this behaviour has been rationalized in the last section. The angular correlation processes have their own independent dynamics localized in the two metallocene fragments.

As a result of the weak π coupling between both monomer units in **1c** and **2c**, it seems of interest to investigate the possibility of a symmetry broken SCF solution where in one metallocene fragment the $3d_{yz}$ AO is highly populated while in the neighbour fused sandwich $3d_{xz}$ has an AO population near $2e$. The relative energies of these broken symmetry solutions are given in the last column of Tables 11 and 12.

It is seen that the charge density wave solution in **2c** is lower (−4.34 kJ/mol) than the symmetry adapted RHF determinant $(3d_{yz})_B/(3d_{yz})_{AB}$. At the first Ni center $3d_{xz}$ is highly populated (about $2e$) while $3d_{yz}$ has a lower value (1.09 e). This ratio is changed at the second $3d$ center. The Wiberg bond indices for the CDW solution of the fulvalene system are displayed on the bottom of Fig. 9. The correspondence to the two symmetry adapted SCF solutions is evident.

In the case of the binickelocene dimer **1c** the CDW solution is 4.16 kJ/mol above the symmetry constrained SCF ground state. Calculations of the singlet instabilities for the broken symmetry solutions of **1c** and **2c** indicate two different localized correlation processes at the two Ni centers. At the first $3d$ atom there is a scattering from $3d_{xz}$ into $3d_{yz}$, while at the second atom $3d_{yz}$ is excited into $3d_{xz}$. A schematical representation of these broken symmetry fluctuations is given in Fig. 12 (for **2c**). The necessary condition for the existence of broken symmetry solutions is the negligible π interaction at the central CC bridge in **1c** and **2c**.

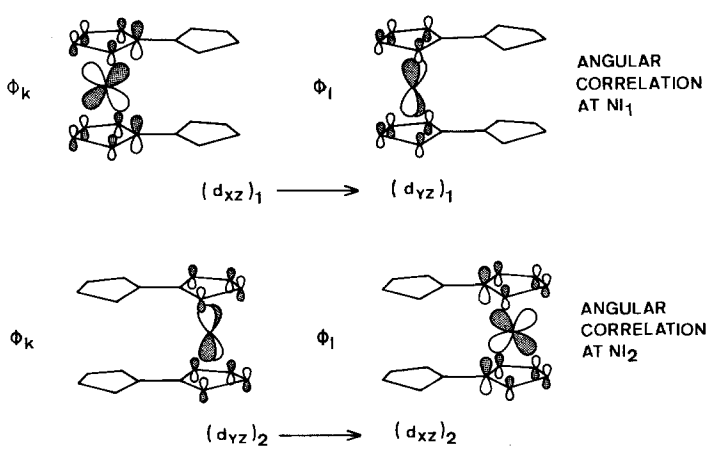

Fig. 12. The two different localized angular correlation processes in the broken symmetry solution of **2c**

The near degeneracy of a symmetry adapted RHF solution and a CDW in **1c** and **2c** suggests that in the case of polynickelocene **4** the existence of a band-structure with a doubled unit cell and a bisected first Brillouin zone has to be taken into account. The two possibilities for the ordering of the $3d$ hole-density (always in $3d_{xz}$, alternating between $3d_{xz}$ and $3d_{yz}$) are shown in Fig. 13. CDW solutions as displayed in Fig. 13 have been detected in some simple model chains [55]. The transition from the symmetrical configuration **4a** to the alternating polymer **4b** reminds us of the Peierls theorem of solid state physics [56]. The existence of a CDW solution in **4** of course has a pronounced influence upon the parameters of the charge carrier dynamics.

The non-singlet (triplet) variations (Tables 13 and 14) in **1c** and **2c** once again differ from the corresponding singlet fluctuations. In both Ni dimers two negative roots are encountered that differ by more than 1.5 eV from the first singlet eigenvalue. The orbital transitions leading to the longitudinal SDW solutions are associated with spin decoupling processes between electron-hole pairs with large $3d_{xz}$ amplitudes. There are two different reasons that lead to an UHF solution due to fluctuations within the $3d_{xz}$ set. In the case of the SCF ground state with the configuration $(3d_{yz})_B/(3d_{yz})_{AB}$ there are no particle-states with significant $3d_{yz}$ amplitudes, while within the $3d_{xz}$ set particle- and hole-states with large metal $3d$ amplitudes are available. Furthermore as already discussed, the central bridge acts as "blocker" for possible long-range interactions for $3d_{yz}$

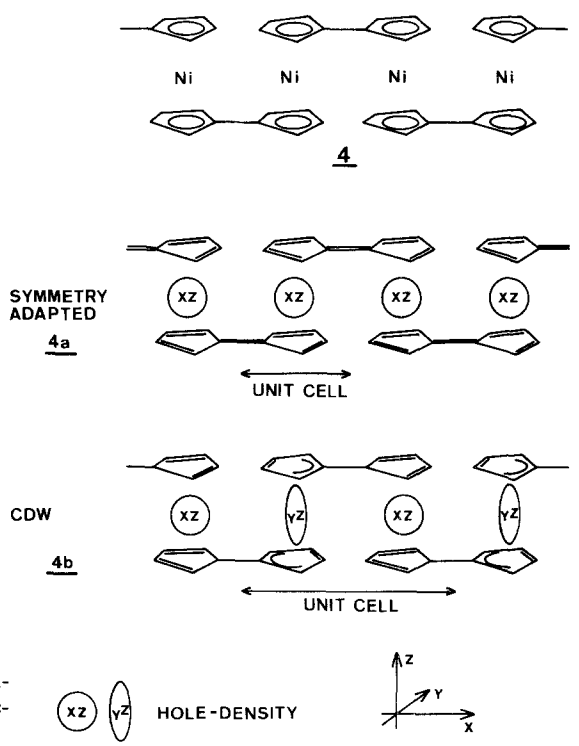

Fig. 13. Comparison between a symmetry adapted and a CDW band-structure in polynickelocene **4**

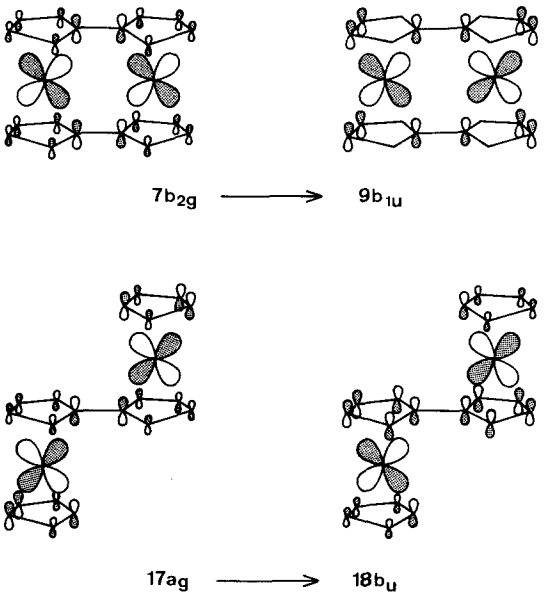

Fig. 14. Schematical representation of the electron-hole pair MOs in **1c** and **2c** leading to the lowest root of the non-singlet instabilities

AOs while long-range coupling via the $3d_{xz}$ functions are transmitted. A schematical representation of the leading terms within the orbital transitions are shown in Fig. 14.

The results for the non-real variations predicted for **1c** and **2c** (Tables 13 and 14) demonstrate the close correspondence between singlet fluctuations of the orbital wave functions and non-real variations.

Table 15. Cr population and net charges of bisfulvalenedichromium **2d** according to an INDO calculation

AO		AO-Population
Cr	$4s$	0.1398
	$4p_x$	0.1194
	$4p_y$	0.1138
	$4p_z$	0.1258
	$3d_{z2}$	0.1359
	$3d_{xz}$	0.8772
	$3d_{yz}$	0.8692
	$3d_{x2-y2}$	1.8346
	$3d_{xy}$	1.8326
Net charges	Cr	−0.0484
	C_1=C_4	−0.1520
	C_2=C_3	−0.1320
	C_{10}	0.0173

Table 16. Results of the singlet and non-singlet instabilities of **2d** according to the INDO method; legend see Table 1

Type	i	λ_i (eV)	$\phi_k \rightarrow \phi_l$	%	MO-Type $_k$	MO-Type ϕ_l	% $3d\ \phi_k$	% $3d\ \phi_l$
Singlet	1	−0.01	$(7b_{3u}) \rightarrow (11a_g)$	45.9	$(3d_{x2-y2})_{AB}$	$(3d_{z2})_B$,	86.7	83.3
			$(9a_g) \rightarrow (9b_{3u})$	35.5	$(3d_{x2-y2})_B$, $L(\pi)$	$(3d_{z2})_{AB}$	70.9	81.7
			$(10a_g) \rightarrow (9b_{3u})$	9.3	$L(\pi)$, $(3d_{x2-y2})_B$	$(3d_{z2})_{AB}$	16.3	81.7
	2	0.00	$(7b_{3u}) \rightarrow (9b_{3u})$	46.3				
			$(9a_g) \rightarrow (11a_g)$	35.0		see $i=1$		
			$(10a_g) \rightarrow (11a_g)$	9.6				
	3	0.10	$(5b_{1g}) \rightarrow (9b_{3u})$	47.3	$(3d_{xy})_{AB}$	$(3d_{z2})_{AB}$	82.7	81.7
			$(5b_{2u}) \rightarrow (11a_g)$	46.8	$(3d_{xy})_B$	$(3d_{z2})_B$	89.4	83.3
	4	0.11	$(5b_{1g}) \rightarrow (11a_g)$	47.3		see $i=3$		
			$(5b_{2u}) \rightarrow (9b_{3u})$	46.8				
Non-singlet	1	−0.04	$(7b_{3u}) \rightarrow (11a_g)$	45.2		see $i=1$		
			$(9a_g) \rightarrow (9b_{3u})$	35.2		singlet		
			$(10a_g) \rightarrow (9b_{3u})$	9.2				
	2	−0.02	$(7b_{3u}) \rightarrow (9b_{3u})$	46.3				
			$(9a_g) \rightarrow (11a_g)$	34.6		see $i=1$		
			$(10a_g) \rightarrow (11a_g)$	9.5				
	3	0.10	$(5b_{1g}) \rightarrow (9b_{3u})$	47.3		see $i=3$		
			$(5b_{2u}) \rightarrow (11a_g)$	46.7		singlet		
	4	0.11	$(5b_{1g}) \rightarrow (11a_g)$	47.3		see $i=3$		
			$(5b_{2u}) \rightarrow (9b_{3u})$	46.7				

8. HF Instabilities in the Bisfulvalene Chromium Complex

The Cr $3d$ AO populations and the net charges of the SCF ground state of bisfulvalenedichromium **2d** are collected in Table 15. Cr $3d_{x2-y2}$ and $3d_{xy}$ are strongly populated (1.83 e), while $3d_{z2}$ has the lowest AO population within the five Cr $3d$ functions. As a result of ligand to metal charge transfer $3d_{xz}$ and $3d_{yz}$ have AO populations of about 0.87 e. Due to the small overlap with ligand orbitals this interaction mechanism separates for $3d_{z2}$. On the basis of the Cr $3d$ occupation no significant differences for the Wiberg indices in the fulvalene ligand are expected. In Fig. 15 the corresponding bond indices are collected. The CC bonds in the five membered rings have comparable values, the π-coupling between both chromocene fragments is small.

In Table 16 the lowest eigenvalues of the singlet and the non-singlet HF instabilities are summarized. The breakdown of the HF picture is clearly recognized. There are strong scattering events between the occupied Cr $3d$ functions $3d_{x2-y2}/3d_{xy}$ and the localized $3d_{z2}$ acceptors. A graphical representation of the orbital excitations leading to the lowest eigenvalues is given in Fig. 16. The Cr $3d$ contribution to the electron-hole MOs exceeds at least 70% and reaches up to 90%. The electron correlation therefore is of intraatomic angular type and is associated with the separated metallocene fragments. In analogy to the

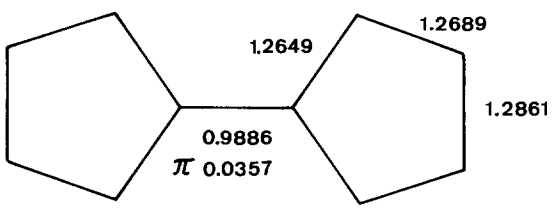

Fig. 15. Wiberg bond indices for the fulvalene ligand in bisfulvalenedichromium **2d**

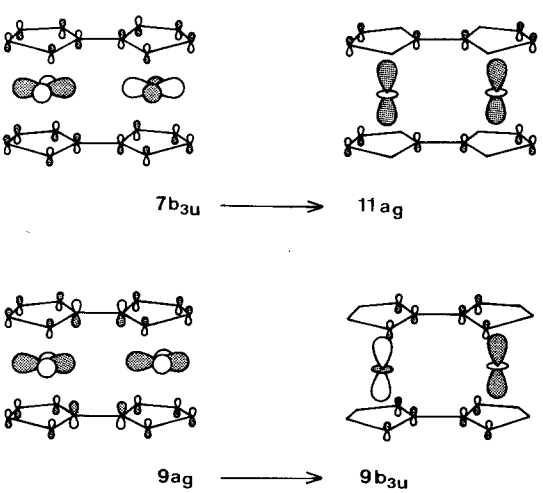

Fig. 16. Schematical representation of the MOs $7b_{3u}$, $10a_g$, $9a_g$ and $9b_{3u}$ contributing predominantly of the first root of the singlet and non-singlet fluctuation

Co and Ni dimers, a left–right correlation does not contribute to fluctuations of the molecular wave function.

In **2d** the necessary condition for dramatical non-singlet fluctuations is not fulfilled (an u/g MO pair with significant Cr $3d$ contributions of the same magnetic quantum number in the hole- and particle-function). The in-phase and out-of-phase linear combinations of Cr $3d$ are either both occupied ($3d_{x2-y2}$, $3d_{xy}$) or both "empty" ($3d_{z2}$, $3d_{xz}$ and $3d_{yz}$). The non-singlet instabilities calculated for this filling scheme correspond to the singlet type excitations. The non-real variations also follow the lines of the singlet problem.

9. Conclusions

The Hartree–Fock instabilities of bimetallocenes and bimetallocenylenes with Fe, Co, Ni and Cr as $3d$ center have been investigated. The synthesized derivatives in the two series **1** and **2** have diamagnetic ground states (α and β spins are paired). It has been demonstrated that the SCF determinant $|\phi_0\rangle$ is a sufficient approximation to the exact ground state only in the case of the d^6 iron dimers **1a** and **2a**. The RHF wave function is stable with respect to violations of the spatial and the spin symmetry and retains its real character.

With an increasing and a decreasing number of $3d$ electrons serious breakdown phenomena of the HF picture are encountered. In the Cr derivative the two $3d_{z2}$ linear combinations of the low lying $3d$ valence orbitals are unoccupied while both (u/g) MOs with large $3d_{x2-y2}$ and $3d_{xy}$ contributions are occupied. The instability calculation shows important intraatomic angular correlation effects between $3d_{x2-y2}/3d_{xy}$ and $3d_{z2}$. The filling scheme of the $3d$ levels in **2d** prevents a further energy lowering due to non-singlet fluctuations.

Pronounced angular correlation effects within the high lying $3d$ functions ($3d_{xz}/3d_{yz}$) suggest the possibility of CDW solutions in the Co and Ni dimers **1b**, **1c**, **2b** and **2c**. The physical origin of this many-body interaction also rests on intraatomic angular correlation. A continued energy lowering due to superimposed left–right correlation is prevented by the central CC bridge in the fulvalene moiety. The singlet fluctuations therefore are of short-range type. This result differs from the correlation pattern in triple-decker sandwich compounds where comparable contributions from the two many-body interactions (angular, left–right) have been detected [21]. The function of an organic bridge between two transition metal centers therefore can be ambident. Depending on the available fragment orbitals correlation processes can be transferred from one $3d$ side to the other or they can be blocked leading to a many-body dynamics in a localized domain (e.g. in the metallocene units).

With respect to the non-singlet variations a significant difference between the Cr dimer and the Co and Ni complexes is diagnozed. In the latter transition metal compounds large negative eigenvalues for the non-singlet instabilities are predicted. The associated orbital transitions correspond to a spin decoupling with an u/g MO pair with pronounced $3d_{xz}$ contributions. Due to the CC-bridge

only a decoupling within $3d_{xz}$ is possible (long-range fluctuation). The spin density wave is modulated in the direction of the longitudinal axis. The necessary condition for the spin decoupling therefore is the existence of an electron-hole pair with large $3d_{xz}$ amplitudes in both MOs (particle- and hole-state). This condition is fulfilled in the Co and Ni systems but not in the bisfulvalene complex of chromium.

The negligible π coupling between the formal fragments has been demonstrated for the Ni compounds **1c** and **2c**; the possibility of symmetry broken solutions has been shown and the consequences for band-structure calculations were mentioned.

The existence of strange solutions for the orbital wave functions (broken symmetry behaviour, CDW, SDW) in discrete polynuclear clusters and infinite chains furthermore points to possible mechanisms of electron and hole transport in mixed transition metal compounds or organometallic conductors and semiconductors. Broken symmetry solutions or localized states demand transport equations by means of adiabatic or non-adiabatic (phonon assisted) electron hopping, phenomenologically introduced both for inorganic [57] and organic [58] polymers. The investigation of the stability of a wave function obtained for a polynuclear cluster or an infinite chain therefore has a bridging function between experimental data, heuristical model assumptions and detailed quantitative ideas concerning the electronic structure of these systems.

Acknowledgment. The author is grateful to the Stiftung Volkswagenwerk for financial support. I warmly thank Mrs. H. Wellnitz and Mrs. I. Grimmer for typing the manuscript.

References

1. Miller, J. S., Epstein, A. J.: Prog. Inorg. Chem. **20**, 1 (1976); Yoffe, A. D.: Chem. Soc. Rev. **5**, 51 (1976); Goodings, E. P.: ibid. **5**, 95 (1976)
2. Hanack, M.: Nachr. Chem. Tech. Lab. **28**, 632 (1980)
3. Krogmann, K.: Angew. Chem. **81**, 10 (1969)
4. Werner, H.: Angew. Chem. **89**, 1 (1977)
5. Siebert, W. in: Advances in organometallic chemistry, Vol. **18**, Stone, F. G. A., West, R., Ed. New York: Academic Press 1980
6. Lorkowski, H.-J.: Top. Curr. Chem. **9**, 207 (1967)
7. Cowan, D. O., LeVanda, C., Park, J., Kaufman, F.: Acc. Chem. Res. **6**, 1 (1973)
8. Ashcroft, N. W., Mermin, N. D.: Solid state physics, New York: Holt, Rinehart and Winston 1976
9. Petrov, E. G.: Int. J. Quantum Chem. **16**, 133 (1979)
10. Anderson, P. W.: Phys. Rev. **102**, 1008 (1958); Anderson, P. W.: Comments Solid State Physics **1**, 190 (1970)
11. Mott, N. F.: Metal-insulator transitions, London: Taylor and Francis 1974
12. Slater, J. C.: Phys. Rev. **82**, 416 (1951)
13. Mott, N. F.: Proc. Roy. Soc. **62**, 416 (1949)
14. Collins, T. C.: Electronic structure of polymers and molecular crystals. Andre, J. M., Ladik, J., Ed. New York: Plenum Press 1975; Collins, T. C. in: Quantum theory of polymers, Andre, J. M., Delhalle, J., Ladik, J., Ed. Dordrecht-Boston: D. Reidel Publ. Co. 1978

15. Ladik, J. in: Recent advances in the quantum theory of polymers, Lecture Notes in Physics, Vol. **113**, Berlin: Springer Verlag 1980
16. Whangbo, M.-H., Hoffmann, R.: J. Am. Chem. Soc. **100**, 6093 (1978); Whangbo, M.-H., Foshee, M. J., Hoffmann, R.: Inorg. Chem. **19**, 1723 (1980)
17. Seelig, F. F.: Z. Naturforsch. **34a**, 986 (1979)
18. Bullett, D. W. in: Solid state physics, Vol. **35**, Ehrenreich, H., Seitz, F., Turnbull, D., Ed. New York: Academic Press 1980
19. Böhm, M. C.: Chem. Phys. Letters, **81**, 284 (1981)
20. Böhm, M. C.: Chem. Phys., in press
21. Böhm, M. C.: Ber. Bunsenges. Phys. Chem., **85**, 755 (1981)
22. Thouless, D. J.: The quantum mechanics of many body systems, New York: Academic Press 1961
23. Whangbo, M.-H.: J. Chem. Phys. **70**, 4963 (1979)
24. Smart, J. C., Pinsky, B. L.: J. Am. Chem. Soc. **99**, 956 (1977)
25. Smart, J. C., Pinsky, B. L.: J. Am. Chem. Soc. **102**, 1009 (1980)
26. Böhm, M. C., Gleiter, R., Delgado-Pena, F., Cowan, D. O.: Inorg. Chem. **19**, 1081 (1980)
27. Böhm, M. C., Gleiter, R.: in preparation
28. Böhm, M. C., Gleiter, R.: Theoret. Chim. Acta (Berl.), **59**, 127 (1981)
29. Čižek, J., Paldus, J.: J. Chem. Phys. **47**, 3976 (1967)
30. Ostlund, N. S.: J. Chem. Phys. **57**, 2994 (1972)
31. Futukome, H.: Prog. Theor. Phys. **47**, 1156 (1972)
32. Chambaud, G., Levy, B., Millie.: Theoret. Chim. Acta (Berl.) **48**, 103 (1978)
33. Löwdin, P.-O. in: Quantum theory of atoms, molecules and the solid state, Löwdin, P.-O., Ed. New York: Academic Press 1966
34. Nakajima, S., Toyozawa, Y., Abe, R.: The physics of elementary excitations, Springer Series in Solid-State Sciences, Vol. **12**, Berlin: Springer Verlag 1980
35. Overhauser, A. W.: Phys. Rev. **128**, 1437 (1962)
36. Kutzelnigg, W.: Top. Curr. Chem. **40**, 31 (1973); Hurley, A. C.: Introduction to the electron theory of small molecules, New York: Academic Press 1976
37. Calculation of vertical ionization potentials in $3d$ complexes by means of the ΔSCF and "Transition Operator" formalism: Böhm, M. C., Gleiter, R., Batich, C. D.: Helv. Chim. Acta **63**, 990 (1980); Böhm, M. C., Gleiter, R.: Z. Naturforsch. **35b**, 1028 (1980); Böhm, M. C., Daub, J., Gleiter, R., Hofmann, P., Lappert, M. F., Öfele, K.: Chem. Ber. **113**, 1028 (1980); Böhm, M. C., Gleiter, R.: Chem. Ber. **113**, 3547 (1980); Böhm, M. C., Gleiter, R.: Comput. Chem. **1**, 407 (1980)
38. Calculation of vertical ionization potentials in $3d$ complexes based on the one-particle Green's function approach: Böhm, M. C., Gleiter, R.: Theoret. Chim. Acta (Berl.) **57**, 315 (1980); Böhm, M. C., Gleiter, R.: Comput. Chem., in press
39. Geometries, excitation energies, atomic populations and net charges of transition metal compounds: Böhm, M. C., Gleiter, R.: Theoret. Chim. Acta (Berl.), **59**, 153 (1981)
40. Kaluski, Z. L., Struckov, J. T., Avoyan, R. L.: Z. Strukt. Khim. SSSR **5**, 743 (1964); McDonald, A. C., Trotter, J.: Acta Cryst. **17**, 872 (1964)
41. Churchill, M. R., Wormald, J.: Inorg. Chem. **8**, 1970 (1969)
42. Haaland, A.: Acc. Chem. Res. **12**, 415 (1979)
43. Fischer, R. D.: Theoret. Chim. Acta (Berl.) **1**, 418 (1963); Schachtschneider, J. H., Prins, P., Roos, P.: Inorg. Chim. Acta **1**, 462 (1967); Shustorovich, E. N., Dyatkina, M. E.: Proc. Acad. of Sciences of the USSR, Phys. Chem. Sect. **128**, 885 (1959); J. Strukt. Chem. (USSR) **1**, 98 (1960)
44. Coutière, M.-M., Demuynck, J., Veillard, A.: Theoret. Chim. Acta (Berl.) **27**, 281 (1972); Bagus, P. S., Wahlgren, U. I., Almlöf, J.: J. Chem. Phys. **64**, 2324 (1976)
45. Evans, S., Green, J. C., Jackson, S. E., Higginson, B.: J. C. S. Dalton (1974) 304
46. Heilbronner, E., Bock, H.: Das HMO Modell und seine Anwendung, Vol. 1, Weinheim (West Germany): Verlag Chemie 1970
47. Kirchner, R. F., Loew, G. H., Müller-Westerhoff, U. T.: Inorg. Chem. **15**, 2665 (1976); Sharp, P. R., Raymond, K. N., Smart, J. C., McKinney, R. J.: J. Am. Chem. Soc. **103**, 753 (1981)
48. Mulliken, R. S.: J. Chem. Phys. **23**, 1833, 2338, 2343 (1955)

49. Wiberg, K. B.: Tetrahedron **24**, 1083 (1968)
50. Kanamori, J.: Prog. Theor. Phys. **30**, 275 (1963)
51. Coulson, C. A., Fischer, I.: Phil. Mag. **40**, 386 (1949); Slater, J. C.: Phys. Rev. **82**, 538 (1951); Goscinski, O., Calais, J.-L.: Arkiv Fysik **29**, 135 (1965)
52. Lozes, R. L., Goscinski, O., Wahlgren, U. I.: Chem. Phys. Letters **63**, 77 (1979)
53. Pauncz, R.: Alternant molecular orbital method, Philadelphia: W. B. Saunders Co. 1967
54. Gutzwiller, M. C.: Phys. Rev. **137A**, 1726 (1965); Friedel, J., Sayers, C. M.: J. Physique **38**, 697 (1977)
55. Kertèsz, M., Koller, J., Azman, A.: J. Chem. Phys. **67**, 1180 (1977); Kertèsz, M., Koller, J., Azman.: Z. Naturforsch. **34a**, 527 (1979)
56. Peierls, R.: Quantum theory of solids, Oxford: Oxford University Press 1955
57. Miller, A., Abrahams, A.: Phys. Rev. **120**, 765 (1960); Mott, N. F., Twose, W. D.: Advan. Phys. **10**, 107 (1961)
58. Gutman, F., Lyons, L. E.: Organic semiconductors, New York: Wiley 1967

Received May 11/July 24, 1981